ASSEMBLY AND PROPULSION OF COLLOIDAL PARTICLES UNDER COMBINED ELECTRIC AND MAGNETIC FIELDS

by

Md. Ashraful Haque

A thesis submitted to the Faculty and the Board of Trustees of the Colorado School of Mines in partial fulfillment of the requirements for the degree of Master of Science.

(Materials Science).

Golden, Colorado

Date _____

Signed: _____

Md Ashraful Haque

Signed: _____

Dr. Ning Wu

Thesis Advisor

Signed: _____

Dr. Angus Rockett

Professor and Head

Department of Metallurgical and Materials Engineering

Golden, Colorado

Date _____

ABSTRACT

Colloids are reminiscent of atoms and molecules with larger dimensions. Under external fields, they tend to get organized in a hierarchical order that shares the same fundamental aspect of functional materials and living organisms. The primary goal of this thesis is to explore the combined impacts of electric and magnetic fields on colloidal assembly and actuation. We first report a strategy combining a planar magnetic field with a one-dimensional electric field to assemble and actuate linear chains made of paramagnetic microspheres. While a horizontal chain lying on the substrate is symmetric fore and aft and does not translate, a two-dimensional magnetic field can tilt the chain with an angle relative to the substrate. A superimposed alternating-current electric field leads to the propulsion of tilted chains along the substrate due to an unbalanced electrohydrodynamic flow. Using the magnetic field for steering and electric field for driving, we reveal a new propulsion mechanism that breaks the symmetry of hydrodynamic flow by manipulating the orientation of a microscopic object. We have also applied electric and magnetic fields orthogonally to magnetic microspheres, which allow us to independently control the magnitude and direction of dipolar attraction and repulsion between the particles. As a result, we obtain various kinds of well-aligned hierarchical structures based on the building blocks of microspheres and colloidal clusters of trimers, tetramers, heptamers, and nonamers. Our results demonstrate the potential in using combined fields to make diversified types of highly aligned structures for applications in high strength composites, optical materials, and battery electrodes.

TABLE OF CONTENTS

LIST OF FIGURES

LIST OF TABLES

LIST OF SYMBOLS

$\psi(x)$ ……Electric potential in solution

ψ_s ……Stern potential

ε_0 ……Permittivity of vacuum

EDL ……Electric double layer

κ^{-1} ……Debye length

K ……Clausius-Mossotti factor

τ_{MW} ……...Maxwell-Wagner relaxation time

D ……Ion Diffusivity

τ_δ ……...Maxwell-Wagner O'Konski relaxation time

τ_α ……...Low frequency dispersion relaxation time

ζ_p ……...Zeta potential

EHD ……...Electrohydrodynamics

θ_c ……...Chain angle

θ_M ……...Magnetic field angle

f_E ……...Electric field frequency

f_M ……....Magnetic field frequency

Pe ……....Peclet number

Du ……Dukhin number

ρ ……Surface coverage

ACKNOWLEDGMENT

My utmost thanks to my advisor, Dr. Ning Wu, to guide me through every corner of this research. It is a privilege for every student to have a mentor like Ning. He has a remarkable way to teach and transcend ideas to the surroundings. I am thankful to Dr. Joseph Samaniuk and Dr. Andrew Petruska. It is my pleasure to have them as committee members. I would like to convey my gratitude to the wonderful research group of Dr. Tao Yang, Dr. Ramona Mhanna, Joseph Maestas, Xingrui Zhu, Yan Gao, Yuanxing Zhang, Nomin Uyanga, Benjamin Hanson, and Isaac Van Tol. Their support has helped me overcome the challenges of this journey. My special thanks to Dr. Tao who made me familiar with synthesis work. I can not but mention of Joseph Maestas, who has continuously shared his insights on simulation. Appreciation to Nomin Uyanga as well for her valuable inputs to my research.

Finally, I am grateful to my family members- my journey is blessed with love and care of Nazia Munir, my parents and my beloved sisters. Their support and sacrifice have brought me where I am today.

“To my Mother”

CHAPTER 1

INTRODUCTION AND LITERATURE REVIEW

1.1 Motivation

Colloids are reminiscent of atoms and molecules with larger dimensions (a factor of 10^2 or more). They can follow the classical nucleation theory in crystallization, which provides valuable insights into phase transitions at the micron scale.[1-2] Under appropriate conditions, they tend to get organized in a hierarchical order that shares the same fundamental aspect of living organisms and functional materials. While both an atom and a colloidal particle can have thermal energy of k_BT (where k_B is Boltzman constant and T is temperature), a three-dimensional (3D) atomic crystal will have a much higher elastic moduli and energy density over their colloidal counterparts. Such lower energies make colloidal systems soft materials, and arguably, give them the benefit of tailorable shapes and sizes. Furthermore, it is possible to induce long-range hydrodynamic interactions in colloid dispersion.[3-4] Because of their relatively larger sizes, they can be studied using conventional optical microscopes. Recent years have witnessed significant efforts in studying model colloidal systems for assembly, crystallization, and active motion.[5-6]

Ever since the fabrication of various types of monodisperse colloidal particles, a wide range of processes and techniques have been developed for making ordered colloidal structures. In recent years, many efforts have been spent to tailor the size, shape, surface property, and interaction of colloids to make dynamically reconfigurable structures exhibiting remarkable optoelectronic properties.[7-8] Essentially, colloids can assemble into crystalline structures by balancing their interparticle forces, a protocol widely known as the self-assembly process. Spherical colloids have been found to form into face-centered cubic (FCC), hexagonal close-packed (HCP), and random HCP structures primarily controlled by thermodynamics.[9-10] The scope of self-assembly can be

further extended by introducing heterogeneous surface chemistry (e.g., on Janus or multiblock particles[11]), adjusting the size ratio in binary systems,[12] and controlling long-range electrostatic interactions.[13] Self-assembly is a powerful bottom-up method for making functional materials and understanding fundamental questions in soft matter physics and materials science. Despite the success in fabricating many novel structures, self-assembly typically suffers from slow kinetics and limited turnability of the inter-particle forces.[14]

Some limitations in self-assembly can be overcome by modulating the effective range, strength, and type of colloidal interactions, which can eventually reduce the assembly time. For example, adding surfactants or using patterned substrates with grooves or channels can tailor the particle-particle and particle-wall interactions.[15-17] The most efficient way is to use external sources such as optical,[18] electric,[19-22] hydrodynamic, acoustic,[23-24], and magnetic fields.[25-28] Sometimes, those fields can also yield an asymmetric distribution of mobile charges or chemicals surrounding the particles. As a result, the concept of active colloids has been popularized. Those colloids can harvest energy from the environment and behave as dynamically re-organized micro/nanomotors.[29-30] The chemical clouds arising from asymmetric surface charge distribution surrounding the particles allow them to interact with neighboring counterparts through phoretic, dipolar, or osmotic forces, consequently introducing out-of-equilibrium behaviors.[31]

This ability to assemble and actuate colloids has allowed researchers to make micro-/nano-machines that can mimic natural systems of macroscopic flocks of living bodies (birds, fishes, ants, etc.) or microscopic swarming of biological cells (e.g., bacteria).[32-33] However, the difficulty associated with the control and coordination of particles' motion at small scales cannot be overlooked. Only a few mechanisms can break the symmetry and reversibility in low Reynolds number (Re) flow. Many efforts have been made to synthesize particles with anisotropic properties

in geometry, interfacial property, or chemical composition. However, such endeavors usually take lots of time and are yet to match expectations. Moreover, the response of particles to any external field can be intricate. There is a great deal of necessity to understand the particle-field interactions and explore alternative external sources capable of guiding particles in a controllable fashion.

The work presented in this thesis is directed to study the behavior of colloidal particles when both electric and magnetic fields are combined. Such an attempt is foreseen to be promising in manipulating colloidal interactions since each field has specific advantages. An electric field can control a wide range of particles (regardless of whether they are dielectric, metallic, or semi-conducting) since most types of particles have a mismatch in dielectric or conducting properties with their dispersing medium. Tuning field parameters such as frequency, strength, and waveform can provide a viable route to controlling field-induced interactions. Furthermore, mobile ions in the solution can also respond to the applied electric field. As a result, electrohydrodynamic flow and the associated interactions, though sometimes complicated, can often arise.

Similarly, the magnetic field also renders many unique features in colloidal assembly. Since magnetic monopoles do not exist, a magnetic field is not screened by "charges", which allows the application of long-range and highly directional magnetic fields required to form complex and large structures. Since magnetic fields can be applied at a distance, it is a genuinely contactless manipulation technique. With the proper selection of wire gauge, proximity losses resulting from eddy currents in Helmholtz coils can be minimized. In addition, the magnetic field strength H_i, frequency ω_i, and phase angle θ_i in each dimension i can all be tuned. Because of this, three-dimensional magnetic fields can be created and manipulated easily. In comparison, the electric field produced in multiple directions interferes with others due to the infinite permittivity of conducting electrodes. As a result, most electric fields are applied in one or two dimensions

only. Furthermore, a magnetic field can penetrate a non-magnetic medium. There is a weak impact of experiment conditions such as temperature, pH, and salt concentration on magnetic interactions, making it applicable to different experimental environments. Depending on the angle between the applied field and the center-to-center line between particles, both electric and magnetic fields can introduce attractive and repulsive dipolar forces. This empowers compelling design freedom. Such highly directional dipolar forces can induce anisotropic interactions even on isotropic particles and lead to fast assembly kinetics (on the order of seconds). Hence, there lies a great prospect in creating multi-axial electric and magnetic fields that take advantage of both fields. This is the primary focus of this thesis.

1.2 Assembly and Active Motion of Colloids Under Electric Fields

1.2.1 The DLVO Theory

The prominent forces involved in colloidal suspensions are dipolar interaction, Van der Waals (VdW) interaction, electrostatic interaction due to overlap of double layers, steric repulsive force arising from adsorbed polymer layers, and solvation force due to interaction of particles with solvent molecules. The Derjaguin, Landau, Verwey, and Overbeek (DLVO) theory is well known for providing paradigm insights on the behavior of colloidal suspensions. The competition between VdW attraction and electrostatic repulsion dictates the states of colloidal stability: dispersed, weakly flocculated, or strongly aggregated. The VdW force between two identical spherical particles with radius R and edge-to-edge separation h can be modeled by[34]

$$U_{vdW} = -\frac{AR}{12h}, \tag{1.1}$$

where the Hamaker constant A is in the range of $10^{-19} - 10^{-21}$J. The VdW force is short-ranged (~5-10 nm), dominant only when particles get close to each other. Consequently, it is safe to neglect the VdW interaction if particles are well-separated.

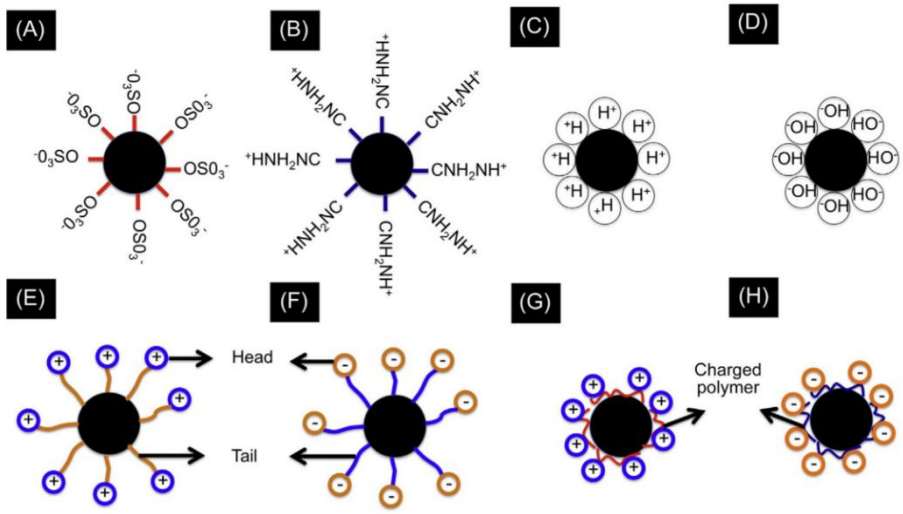

Figure 1.1 Different mechanisms that introduce charges on a particle surface: dissociation of covalently attached chemical species (A, B), adsorption of ions (C, D), surfactant molecules (E, F), charged polymers, and polyelectrolytes (G, H).35 Reprinted with permission from ref [35]. Copyright 2012, Cambridge University Press.

When a particle is suspended in a polar solvent such as water, surface charges can develop via mechanisms such as (1) dissociation of neutral surface functional groups into charged groups and mobile ions in solution, (2) Nernstian charging through specific absorption/desorption of ions, (3) protonation/deprotonation of acidic or basic surface groups, and (4) incongruent dissolution (leaching).[36] For example, a latex particle functionalized with carboxylic groups becomes negatively charged via mechanism (1) at pH 7. Since the system (both charged particle and the surrounding mobile ions) is neutral, the developed surface charges would be partially compensated by counterions through adsorption within a very thin layer next to the particle known as the Stern layer. There would be another layer for the electrostatic accumulation of counterions known as the

Gouy-Chapman (GC) layer outside the Stern layer. Consequently, the electric potential $\psi(x)$ in the solution varies exponentially:[34]

$$\psi(x) = \psi_s e^{-\kappa x}, \tag{1.2}$$

where ψ_s is the Stern potential, κ^{-1} is the Debye length, and x is the distance from the particle surface. When two particles are close to each other, their GC layers overlap and the resulting increment of counterion concentration between them, in turn, leads to a repulsive electrostatic interaction. For two identical spheres with radii R being separated at distance h, this double layer interaction can be calculated by[34]

$$U_{EDL}(d) = 2\varepsilon\varepsilon_0 R{\psi_s}^2 e^{-\kappa h}, \tag{1.3}$$

where ε and ε_0 are dielectric constant of medium and permittivity of vacuum, respectively.

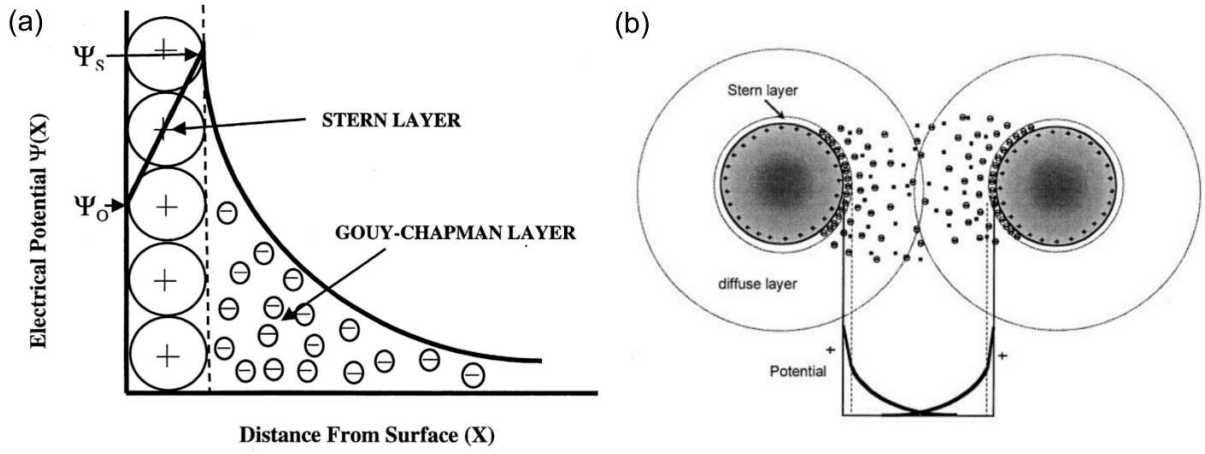

Figure 1.2 (a) Electrical double layer (EDL) near a charged surface with a Stern layer of positive ions adsorbed to the surface. (b) Overlapping EDL causes electrostatic repulsion.[34] Reprinted with permission from ref [34]. Copyright 2001, Elsevier: Oxford.

Combining the VdW attraction and electric double layer repulsion, one can obtain the so-called DLVO interactions (Figure 1.3) between particles. It can be seen that a large particle surface potential creates an energy barrier that prevents the system from reaching the primary minimum. On the other hand, if the surface potential is small, it would be much easier to overcome the energy

barrier. The existence of the primary minimum close to the contact of particles characterizes an aggregation state. In some instances, there is a secondary minimum in the DLVO curve which indicates weak agglomeration.

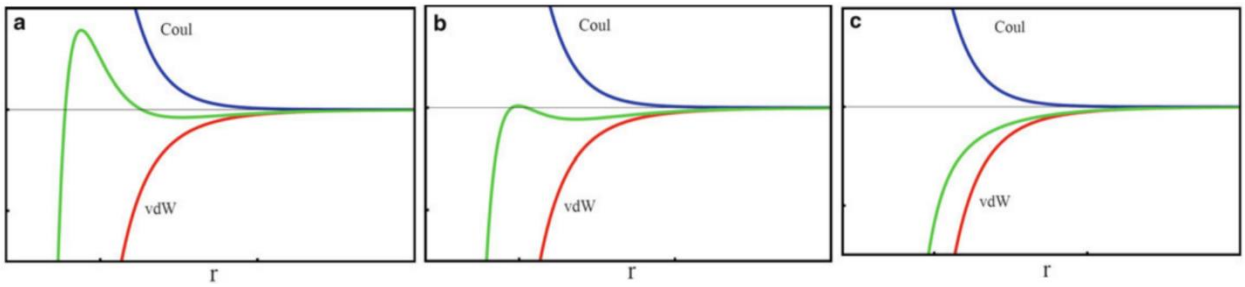

Figure 1.3 The resultant DLVO interaction energy between colloidal spheres.[37] Reprinted with permission from ref [37]. Copyright 2014, Springer New York.

The ion concentration in solvent controls the range of the electric double layer (EDL) interactions by influencing the Debye length. For instance, increasing salt concentration will reduce κ^{-1} making double layers more compressed. As a result, the range of EDL interaction becomes smaller, so VdW interaction could dominate and cause particle aggregation. In contrast, particles will have a net repulsion at low ion concentrations if they are separated far enough. The competition between VdW and EDL interactions has successfully explained the stability of colloidal suspensions. In addition to electrostatic repulsion, colloidal suspensions can also be stabilized by a combined effect of electrostatic and steric hindrance, known as the electrosteric stabilization,[38] induced by the adsorbed polyelectrolytes (Figure 1.4).

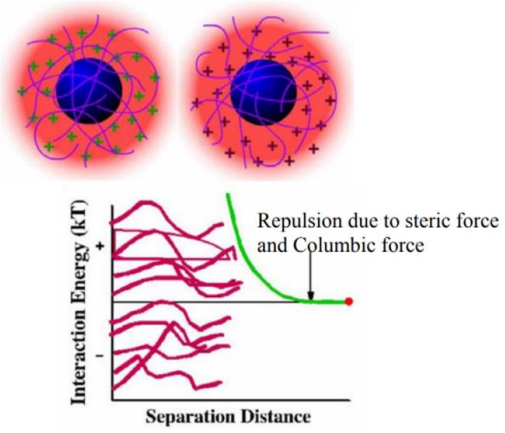

Figure 1.4 Colloidal stabilization through the electrosteric mechanism.[38-40] Reprinted with permission from ref [38]. Copyright 2002, American Chemical Society.

1.2.2 Dipolar Interaction between Particles

A particle can act as a point dipole under an externally applied electric or magnetic field. For example, when an electric field $E = E_0\cos(wt)$ (where E_0 is applied electric field strength and ω is the angular frequency, respectively) is applied, mobile ions in the electric double layer (EDL) will redistribute to two opposite poles of the particle through migration, convection, and diffusion.[41] The movement of those ions remains out of phase to the applied field. Consequently, the effective dielectric constant of both particle and medium can be expressed in the form of complex permittivities $\varepsilon_p^* = \varepsilon_p + \sigma_p/i\omega$ and $\varepsilon_m^* = \varepsilon_m + \sigma_m/i\omega$, respectively, where σ_p (σ_m) is the conductivity of the particle (medium). The combined effect of particle and medium properties can be incorporated into the so-called Clausius-Mossotti factor $K = \frac{\varepsilon_p^* - \varepsilon_m^*}{\varepsilon_p^* + 2\varepsilon_m^*}$. Such a formula lays the foundation of the polarization theory, relating properties of particles, medium, and external fields to the induced dipole of a particle. It is noted that neutral particles dispersed in non-polar solvents do not have EDL and they simply get polarized due to a mismatch of the dielectric

constants between the particle and the medium. The polarization of particles dispersed in an aqueous or polar solvent is dictated by the movement of ions and their corresponding relaxation time scales. Depending on the applied field frequency, there are two types of particle polarization mechanisms based on the Maxwell-Wagner-O'Konski (MWO) and Dukhin-Shilov (DS) theories. When the electric field frequency is high, the migration of ions, in and out of the electric double layer, cannot follow the change of field polarity, resulting in the so-called Maxwell-Wagner (MW) charge relaxation time $\tau_{MW} = \frac{\varepsilon_p + 2\varepsilon_m}{\sigma_p + 2\sigma_m}$, which also identifies the crossover frequency for dielectrophoresis (DEP).[42] For dielectric particles, τ_{MW} can be on order of the electrolyte relaxation time $\tau_D = \kappa^{-2}/D$, where D is the ion diffusivity and $\kappa^{-1} = \sqrt{\varepsilon_m kT / 2z^2 e^2 c N_A}$ with c being the ion concentration, e electron charge, and N_A the Avogadro number. For $\kappa^{-1} = 1 - 100\ nm$, $D = 10^{-9}\ m^2/s$, $1/\tau_{MW}$ ranges from 100 kHz to 1 MHz. The right bound of this regime can be further modified by O'Konski leading to the MWO theory by accounting for the surface conductivities of charged particles based on migration and convections of ions[43] with characteristic time $\tau_\delta = \varepsilon_p \varepsilon_0 + 2\varepsilon_m \varepsilon_0 / (\sigma_p + 2\sigma_m)$. Here, both conductivities from the bulk (σ_p^b) and the surface (σ_p^s) contribute to the effective particle conductivity σ_p, which can be higher than the medium conductivity σ_m, especially for high zeta potentials. At much lower frequencies, both counter- and co-ions have sufficient time to move to two opposite poles of the particle, leading to a macroscopic polarization of the double-layer. Consequently, the diffusion flux from the surrounding bulk fluid and the electro-migration flux of ions within the EDL will counter-balance to reach equilibrium.[44] This low-frequency dielectric dispersion (LFDD) model is based on the Dukhin-Shilov (DS) theory, where diffusion of ions across the particle creates variable double-layer thickness.[45] LFDD has a relaxation time $\tau_\alpha = a^2/D$, where a is the particle radius.

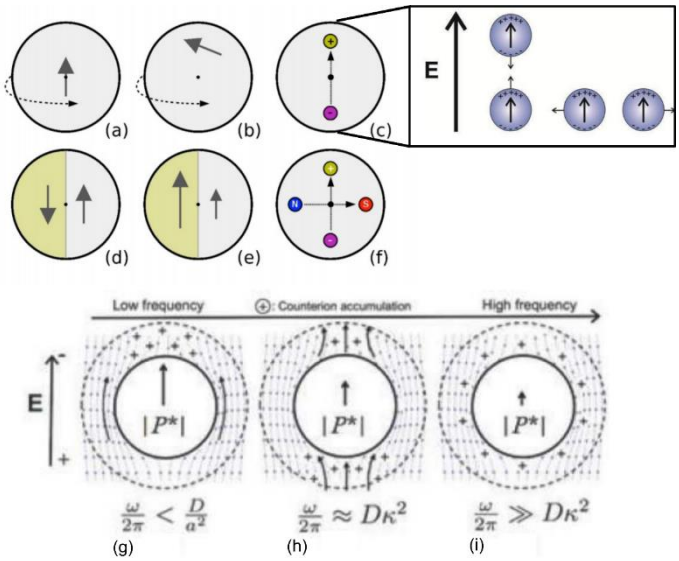

Figure 1.5 Dipolar ((a)-(c)) and multipolar ((d)-(f)) interactions of colloids. (a) The permanent dipole moment of a hard or soft sphere in its center. (b) Point dipole that is shifted laterally from the center where dipole moment is perpendicular from the radius. (c) Permanent or induced dipole from two charges. There will be attraction along with head-tail arrangement and repulsion along shoulder-shoulder. (d) Induced point dipole for Janus-like spheres. (e) Induced parallel point dipole for Janus like a sphere. (e) Two crossed, electric and magnetic, dipoles induced by bi-directional fields.[46] Reprinted with permission from ref [46]. Copyright 2016, Elsevier.((g)-(i)) Different arrangements of ion fluxes around a colloidal particle upon the application of an AC electric field with different frequencies.[47] Reprinted with permission from ref [47]. Copyright 2016, Colorado School of Mines.

The effect of these different polarization mechanisms at different frequency regimes is reflected in the polarization coefficient *K*. At higher frequencies $K = (\varepsilon_p - \varepsilon_m)/(\varepsilon_p + 2\varepsilon_m)$, indicating that the dipole direction is dictated by the dielectric contrast between particle and medium. When frequency gets lower, a dielectric particle can have a larger surface conductivity than the medium conductivity. A non-monotonic dependence of the polarization coefficient on frequency has been observed.[48] Another important insight is how zeta potential (ζ_p) impacts the induced dipole direction. In general, ζ_p is an indicator of the number of surface charges on a particle. A neutral dielectric particle with zero ζ_p in a polar solvent will have an antiparallel dipole

(to the applied field) with negative K. With increasing ζ_p, the surface conductivity of particles will increase due to more polarized ions around the particle. It is possible for a particle with a certain large ζ_p to be more polarizable than the medium. It should be noted that ions in both diffusive and Stern layers can contribute to the particle surface conductivity. A recent study by Yang et al. [49] has shown opposite dipoles for two types of particles with almost the same ζ_p but quite different Stern-layer conductivities.

With the point-dipole approximation, the dipolar force between two identical spheres can be expressed by[45]

$$F_E^d = \frac{3}{4}\pi\varepsilon_m a^2 \left|K^2\right| E_{rms}^2 \left(\frac{2a}{r}\right)^4 [3\cos^2\theta - 1]\hat{r} + (\sin 2\theta)\theta], \tag{1.4}$$

where θ is the angle between particles' center line and the applied field direction, E_{rms} is the root mean squared magnitude of the applied electric field, r is the center-to-center separation between particles and $|K|$ is the magnitude of the polarization coefficient.

Similarly, under an external magnetic field, a magnetic dipole can be induced on a magnetic particle due to both the applied field, **H**, and the dipolar field generated from its neighboring particles, $\mathbf{H}_d$. The magnetic dipole moment would be $\mathbf{m}_{total} = m_r\hat{\mathbf{r}} + m_n\mathbf{n}$, where $\hat{\mathbf{r}}$ is the unit vector connecting the centers of the particles and $\mathbf{n}$ is the unit vector normal to $\hat{\mathbf{r}}$. For two spherical particles, the induced field $\mathbf{H}_d = \frac{1}{4\pi r^3}(2m_r\hat{\mathbf{r}} - m_n\mathbf{n})$ will result in the magnetic moment

$$\mathbf{m}_{total} = \frac{4}{3}\pi R^3 \chi_{eff}\left[\frac{1}{4\pi r^3}(2m_r\hat{\mathbf{r}} - m_n\mathbf{n}) + \mathbf{H}\right] \text{ and} \tag{1.5}$$

$$\chi_{eff} = 3\frac{\mu_p - \mu_m}{\mu_p + 2\mu_m}, m_r = \frac{\frac{4}{3}\pi R^3 \chi_{eff} H\cos\theta}{1 - \frac{2}{3}\chi_{eff}(R/r)^3}, m_n = \frac{\frac{4}{3}\pi R^3 \chi_{eff} H\sin\theta}{1 + \frac{1}{3}\chi_{eff}(R/r)^3}, \tag{1.6}$$

where χ_{eff} is the effective particle susceptibility, μ_p is the particle permeability, and μ_m is the medium permeability. Consequently, the pair interaction between two magnetic spheres is[50]

$$U_{mag} = \frac{m^2 \mu_m}{4\pi r^3} \frac{1}{1-\frac{2}{3}\chi_{eff}(R/r)^3} \left[1 - 3\cos^2\theta + \left[\frac{1-\frac{2}{3}\chi_{eff}(R/r)^3}{1+\frac{1}{3}\chi_{eff}(R/r)^3} \right]^2 \sin^2\theta \right] \tag{1.7}$$

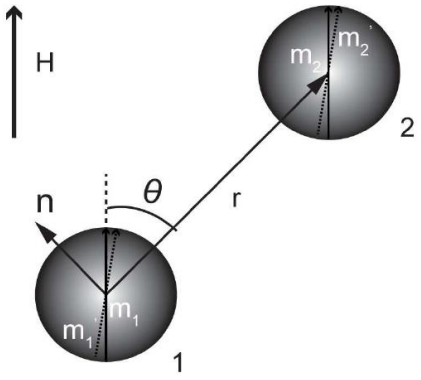

Figure 1.6 Schematic of the dipolar interaction between two spheres. The permanent dipole is indicated by the solid lines, while the dashed lines represent induced dipoles.

1.2.3 Electrohydrodynamic Flow

In addition to dipolar interactions, the application of a DC or AC electric field could also induce the movement of ions in the solution, which drags water molecules with them. As a result, electrohydrodynamic (EHD) flow can be generated. Much of the insight on EHD flow originated from earlier investigations of electroosmosis (EO) and electrophoresis (EP). Both phenomena were first observed by Reuss in 1809.[51] Excess counterions within the Debye layer respond to a longitudinal electric field, inducing fluid flow within a channel and this flow is known as electroosmosis. Similarly, a charged particle can translate under an electric field that gives rise to observation of electrophoresis.

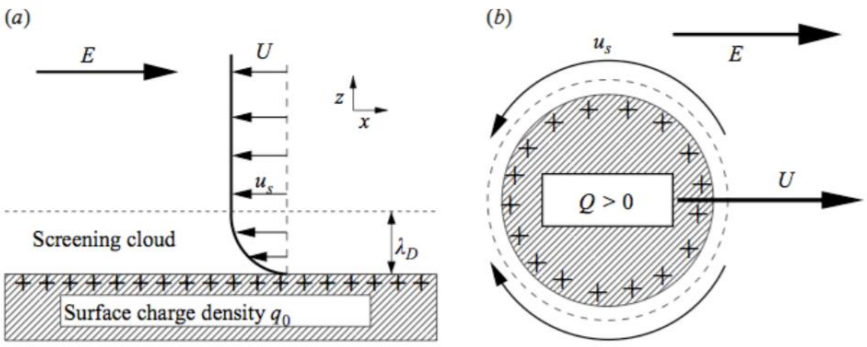

Figure 1.7 (a) Screening cloud of excess counter ions forms a capacitor within the diffusive layer. Applied tangential electric field drives flow parallel to the surface with a slip velocity outside the double layer. (b) When a particle with thin double layers is suspended in an electrolyte, the electroosmosis near the particle surface will cause particle motion known as "electrophoresis".[52] Reprinted with permission from ref [52]. Copyright 2011, Springer Nature.

When a particle near an electrode is subject to a DC electric field applied perpendicular to the substrate, equilibrium ions in the Debye layer respond to the field and generate an electroosmotic flow along the particle surface. This so-called equilibrium-charge electroosmosis (ECEO)[53] generates lateral electrohydrodynamic flow, which causes particle aggregation or segregation depending on the sign of the particle zeta potential and polarity of the electric field. Since ECEO is a linear electrokinetic phenomenon, the time average of this electroosmotic flow should be zero under an AC electric field. However, a net electroosmotic flow was also observed for particles under AC electric fields. The particles were found to undergo periodic oscillation in the vertical direction when it is near a conducting substrate and there exists a phase angle θ between the particle oscillation and the applied AC electric field. However, the origin of this phase angle remains elusive.[54]

One explanation of the electroosmotic flow observed under AC electric fields is the induced-charge electroosmotic flow (ICEO) that usually occurs near ideally polarizable (e.g., metallic) surfaces whose electrostatic potential is held constant. Electrons in metal drift from one

pole to another with the field application, generating ionic currents in the solution, which attract counterions on the opposite poles. The accumulation of counterions (induced charges) effectively charges the double layer like a capacitor until the field lines are expelled from the metal surface. Eventually, the tangential component of the applied field acts on the induced charges and drives a quadrupolar ICEO flow around the particle surface, as shown by Figure 1.8.

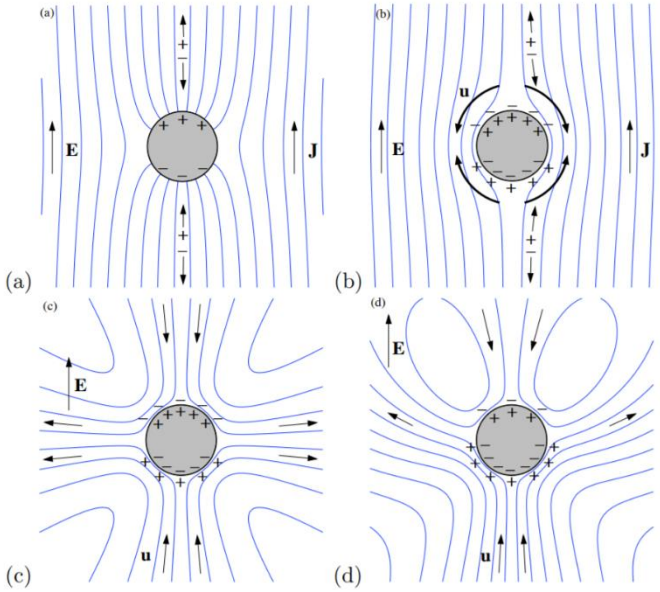

Figure 1.8 (a) Charging of the double layer. (b) Induced charges in the double-layer expells the field lines when a sudden DC field is applied. (c) Quadrupolar ICEO flow is initiated by a tangential field acting on the induced charges. (d) The superimposed flow of linear electrophoresis (ECEO) and quadrupolar ICEO.[52] Reprinted with permission from ref [52]. Copyright 2011, Springer Nature.

When a dielectric particle is adjacent to a conducting electrode, a similar electrohydrodynamic (EHD) flow can also lead to the aggregation or segregation of particles under a perpendicularly applied AC electric field.[55] Since the electrode is conducting, the applied field polarizes it and induces excess ions within the double layer near it. Those ions, however, can only move in the direction perpendicular to the substrate if there is no particle nearby. When a particle

is adjacent to the electrode, it will also respond to the applied field via the polarization of its dielectric core and its double layer. The polarized particle will generate an electric field, and its tangential component will drive the lateral motion of induced charges along the substrate. As a result, an EHD flow ensues. Since the applied field induces both mobile ions near the electrode and a dipole on the particle, the EHD flow velocity is proportional to the field strength squared and inversely proportional to the angular frequency of the field, i.e. $u_{EHD} \propto E_0^2 / \omega$.[56] Depending on the nature of the EHD flow (contractile vs. extensile, as shown in Figure 1.9), particles will experience hydrodynamic attraction or repulsion, which causes the formation of close-packed crystals or segregation of particles into non-close packed arrays. The EHD flow surrounding spherical particles was investigated theoretically and experimentally by Ristenpart et al.[57] It was later explored extensively by Ma et al.[58] for different kinds of asymmetric colloidal particles.

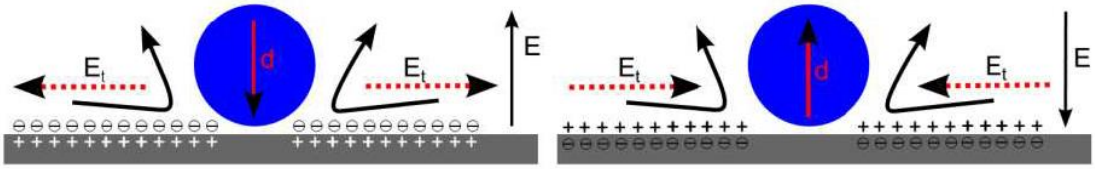

Figure 1.9 EHD flow surrounding a spherical particle under two half periods of an AC electric field.[58] Reprinted with permission from ref [58]. Copyright 2015, Colorado School of Mines.

Oils or non-aqueous solvents, when used as a medium, are found to exhibit another type of EHD flow. Due to their weak conductivity, charges accumulate at the interface between particle and solvent. Taylor's oil droplet experiments under an electric field are known for this phenomenon. The applied field pulls the accumulated surface charges and creates quadrupolar vortices both inside and outside the droplet. As a result, the droplet not only deforms but also

moves under the realm of EHD whose motion varies as $u_{Leaky} \propto E^2 a$.[59] It is important to note that if a solid particle instead of a liquid droplet is used, there would be no net EHD motion. In such a medium, the electric field significantly lowers the amount of current that can induce at the fluid/fluid interface. The author himself investigated this realm in his previous studies to drive various kinds of droplets with different dielectric properties and pump viscous liquids, where high voltage gas discharge was used as a contactless electric field source.[60]

Dielectric liquids containing additives are found to alter the behavior of EHD significantly. So far, for the systems mentioned above, conductivity is typically assumed to be constant. However, the electrical conductivity of a liquid can be substantially increased due to perturbation of dissociation-recombination equilibrium, an effect known as the Onsager effect.[61] When a particle gets polarized near a conducting substrate under a vertical AC electric field, the fluid flow velocity induced from this conductivity gradient was found to scale with the field strength cubed, i.e., $u \propto E_0^3$.[62]

1.3 Colloidal Assembly under Magnetic Fields

The simplest ordered state for an ensemble of colloidal particles under a uniaxial DC or AC magnetic field is one-dimensional (1D) colloidal chains aligned parallel to the external field.[63-64] The strength of intrachain attraction and interchain repulsion can be enhanced by increasing the particle concentration, where neighboring chains can further aggregate into zigzag bundles, 2D sheets, or labyrinth structures that maximize the dipolar attractions between particles[26, 65-66]. However, the use of multi-axial magnetic fields where phase angles or frequencies along each direction are different can significantly extend the range of particle interactions, thus yielding more complex and intriguing structures. For example, a biaxial and planar rotating field along the substrate can induce isotropic attraction between colloidal particles that leads to close-packed

hexagonal arrays.[67-68] A biaxial field can be further modified into a triaxial field by adding a vertical component along the *z*-axis. In a balanced triaxial field (BTF) where all three components' field strengths have the same amplitudes, a van der Waals type interaction between a pair of colloids that scales with r^{-6} can be predicted theoretically. As a result, one might expect homogeneous aggregation of particles just like their molecular counterparts. However, complex structures such as networks, foams, and colloidal clusters have been observed.[69] This is caused by the many-body interactions where particles are polarized not only by the applied field but the polarization field of other particles.

A multi-axial field combining both electric and magnetic components is a somewhat new avenue. Under an electric field, dipoles are induced by the combined polarization of particles, their surrounding double layer, and the solvent. In contrast, the polarization of the magnetic domain within particles leads to the magnetic dipoles under a magnetic field. Some attempts have been made to generate a network of off-centered magnetic colloids under a concurrent planar arrangement of electric and magnetic fields where the substrate plays a vital role in dipolar interactions.[70] Currently, the superposition of electric and magnetic fields remains largely unexplored, although it may allow better control over alignment and spatial distributions of particles.[71]

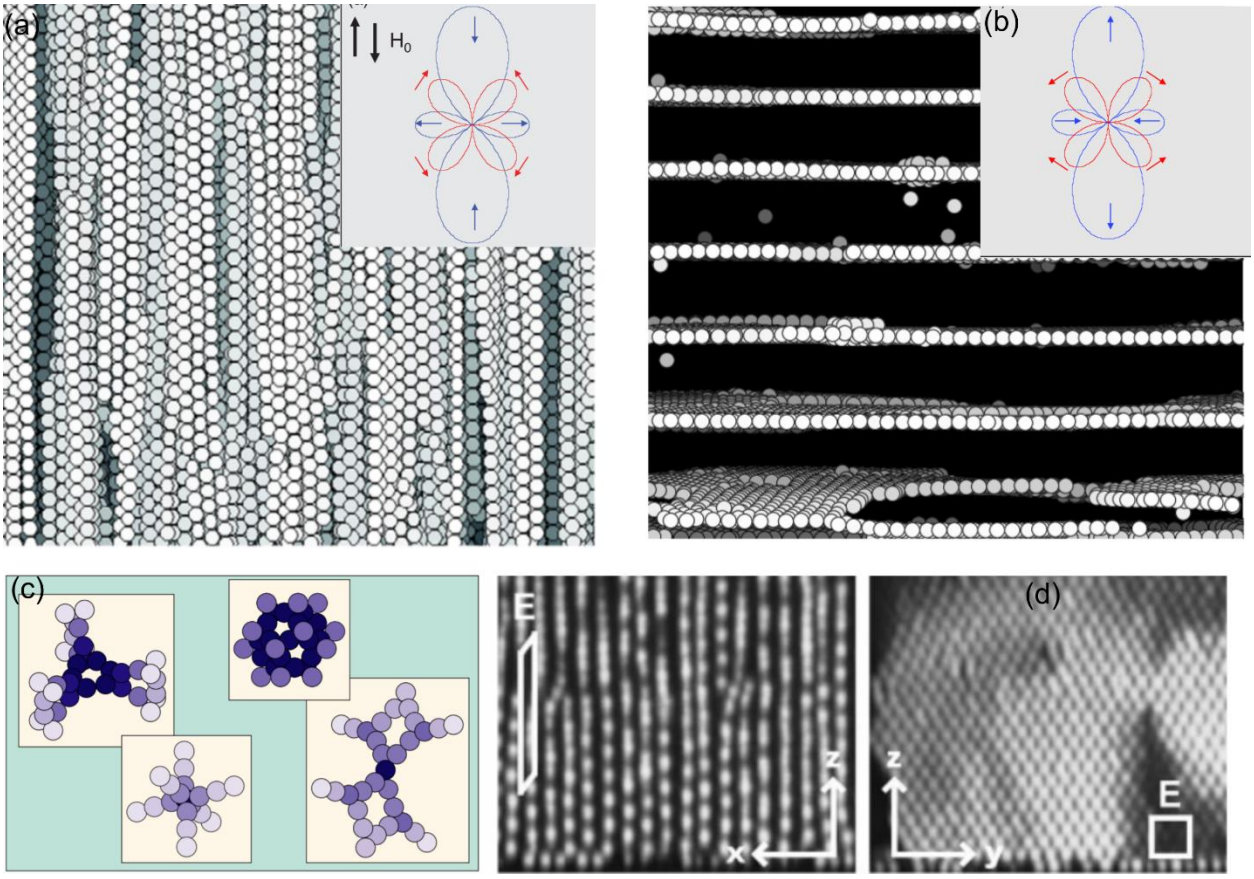

Figure 1.10 Colloidal structures formed under (a) a uniaxial, (b) biaxial, and (c) triaxial field. The insets show different dipolar interactions between two particles.[72] Reprinted with permission from ref [72] Copyright 2013, IOP Publishing, Ltd (d) Colloidal structures formed under a randomly rotating electric field.[67] Reprinted with permission from ref [67]. Copyright 2017, Springer Nature.

In addition to a single component, the particle interactions, hence, structures, can be tuned over a wide range by using a binary mixture of particles of different sizes and material properties. For example, complex structures such as flowers, rings, and honeycombs have been reported by combining superparamagnetic particles with diamagnetic particles in ferrofluids (fluids containing magnetic nanoparticles) in which both positive and negative dipoles can be induced in the same system.[73-75]

1.4 Systems of Active Matter

An active matter system can transduce energy from the environment into motion and is often characterized by its non-equilibrium behavior. Many natural systems ranging from human crowds to bacterial colonies exemplify this aspect. Similarly, colloidal systems can be driven out of equilibrium, especially when hydrodynamics is involved. Examples of active colloids include platinum-coated Janus microspheres in dilute hydrogen peroxide solution,[76] polystyrene dimers driven by EHD or ICEP,[21] particles in a mixture of water and lutidine,[77] and Quincke rollers under DC electric fields.[78] Usually, an equilibrium structure is determined by the balance of potential energy and entropy, leading to free energy minimization. In comparison, non-equilibrium systems typically involve continuous energy input that is dissipated by their constituents. A subject of interest is how collective dynamics emerge in these non-equilibrium systems driven by external fields.

Some recent studies have demonstrated that an ensemble of colloids can interact and translate under an asymmetric ratchet potential created on the substrate (Figure 1.11). If an AC driving force is applied on a particle located within asymmetric potential, it will just rock back and forth without any net translation. However, as soon as the potential becomes asymmetric, interesting dynamics initiate. In the absence of thermal fluctuations, if the maximum pinning forces exerted by the substrate on the particle along $+x$ and $-x$ directions are f_{+m} and f_{-m}, respectively, an AC driving force, $f_{ext} = f_0 \sin(wt)$, can drive the particle in specific directions by making $f_0 > f_{+m}$ or $f_0 > f_{-m}$. Such an asymmetric and periodic potential landscape was created in ferrite garnet films (FGF). By applying an external time-dependent field, the particles can be forced to synchronize with the traveling wave landscape of the FGF film.[79]

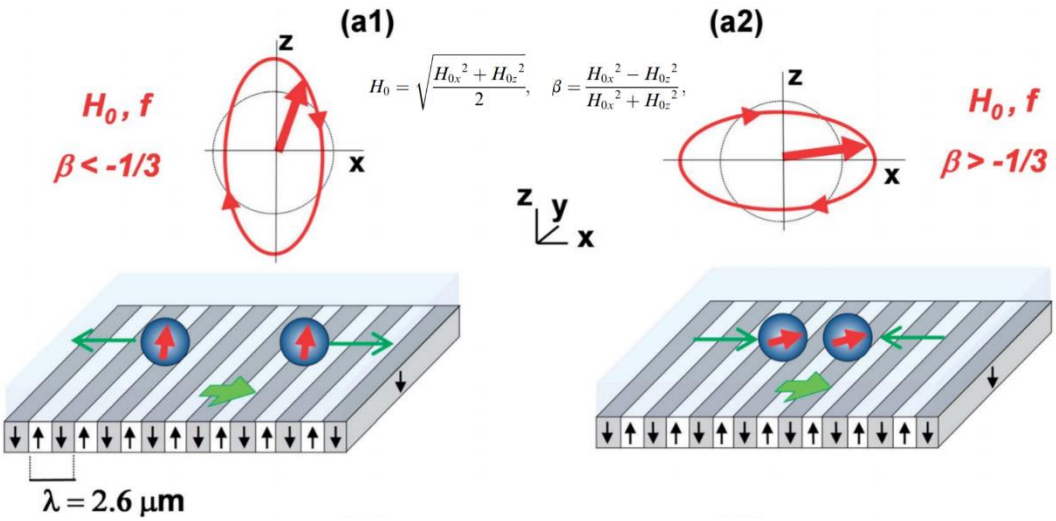

Figure 1.11 Paramagnetic particles on a ferrite garnet film (FGF) substrate. The particles experience either repulsive (a1) or attractive (a2) interactions induced by a rotating magnetic field with elliptic polarization. The attraction leads to the formation of doublets which translate collectively due to the interplay between the substrate and the external field.[79] Reprinted with permission from ref [79]. Copyright 2014, The Royal Society of Chemistry (RSC).

The collective behavior of swimmers described at the beginning of Section 1.4 represents an emerging research topic.[80] Theoretical and experimental development of some artificial swimmers and the associated propulsion mechanisms have been reviewed in Sections 1.1 and 1.3. The standard model for studying those self-propelling objects in Stokes flow is the so-called "squirmer" model: spheres with prescribed tangential velocity profiles on their surfaces. This model can describe the motion of swimmers, both in bulk and close to the substrate. Different kinds of phoretic or catalytic forces of electric, magnetic, photonic, or acoustic origins can create those tangential velocity profiles for swimmers of both isotropic and anisotropic shapes mentioned above.

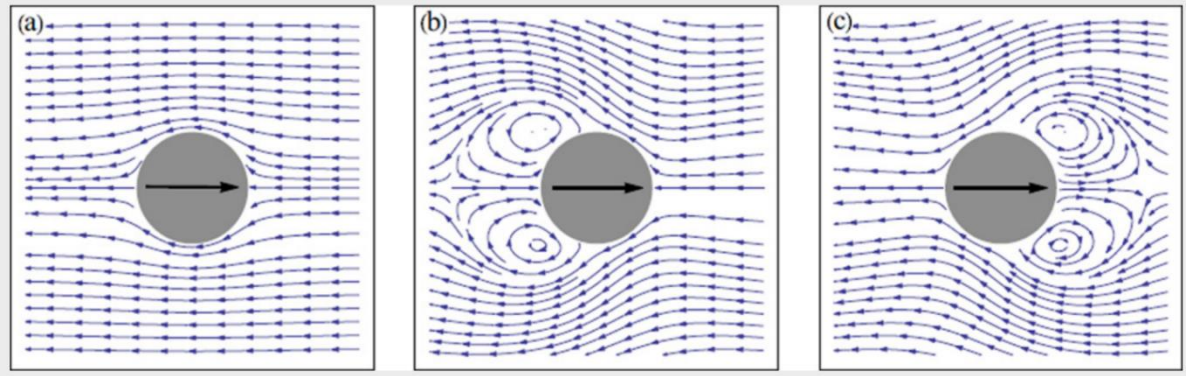

Figure 1.12 Streamlines around squirmers: (a) neutral, (b) puller, and (c) pusher.[81] Reprinted with permission from ref [81]. Copyright 2014, Springer Nature.

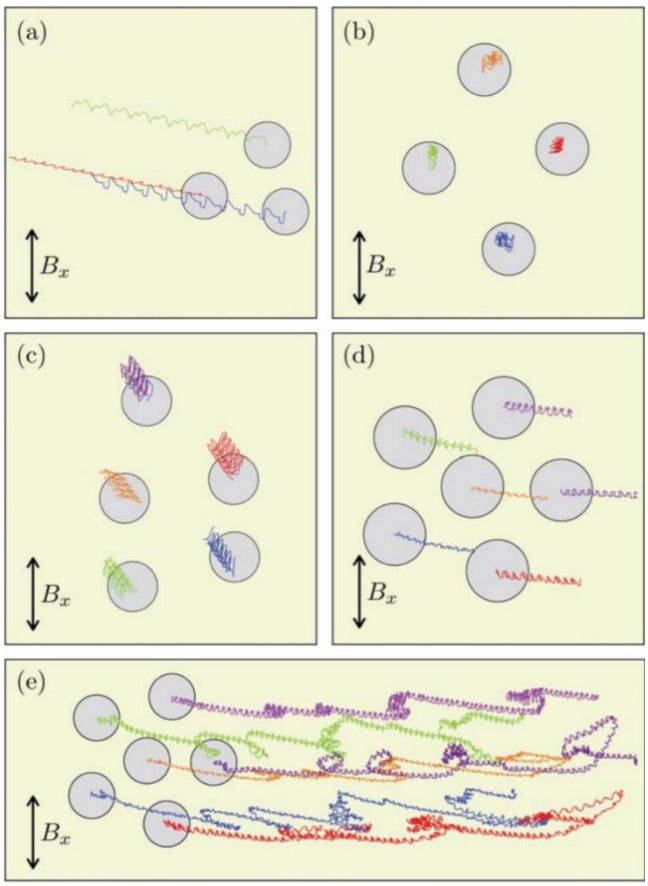

Figure 1.13 An oscillating magnetic field applied along the *x*-direction leads to the formation and collective motion of colloidal clusters.[82] Reprinted with permission from ref [82]. Copyright 2013, The Royal Society of Chemistry (RSC).

For one instance, the interaction amongst the swimmers, light-activated hematite cubes, causes them to aggregate into crystal-like clusters via phoretic attractions.[82] When periodic deformations were introduced, particles within the assembly moved cooperatively under an oscillating magnetic field. One fascinating demonstration of the collective behavior of active matter is the mesoscopic turbulence seen in bacteria's swarms, flocking of birds, and human crowds in panic. Researchers have speculated whether any microscopic interactions such as the hydrodynamics interactions can lead to turbulent states and have shown that they can exist for active rods with a specific range of particle aspect ratios, as seen in Figure 1.14. Interestingly, this kind of turbulence was also experimentally realized for dense suspensions of Janus particles propelling under an AC electric field.[83] A remarkable observation is the "lane" formation which has been viewed as an example of non-equilibrium self-organization processes. Investigations on charged colloids revealed the fundamental impacts of hydrodynamics, particle concentrations, dynamical locking, and anisotropic frictions on lane formation.[84-86]

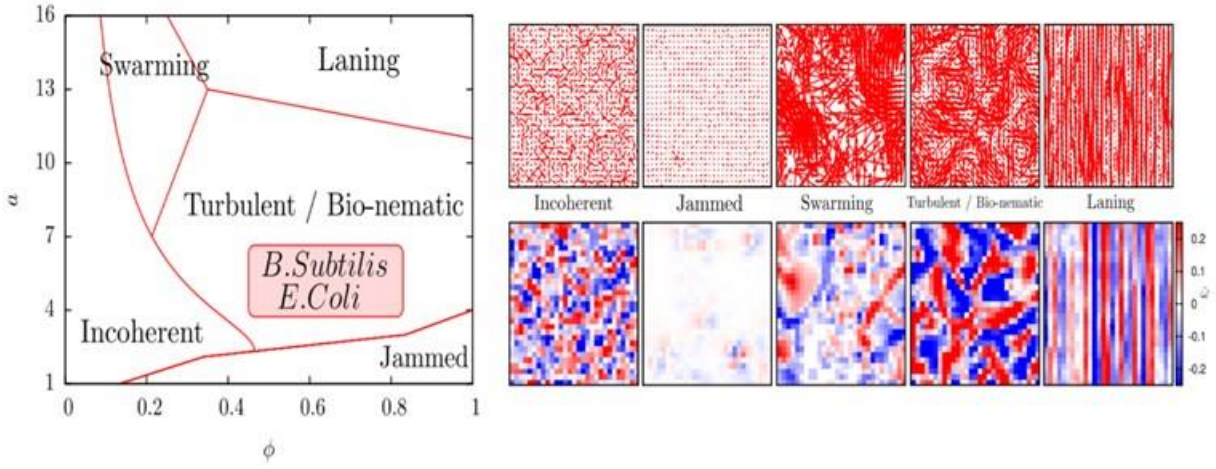

Figure 1.14 Non-equilibrium "phase" behavior of active rods based on (a) particle aspect ratio (a) and (b) concentration (ϕ).[87] Reprinted with permission from ref [87]. Copyright 2012, IOP Publishing.

1.5 Summary

Applying external fields to colloidal suspension can result in various kinds of complex structures and model systems of active matter. Current studies, however, primarily focus on the response of colloids under specific types of external fields. The synergistic impacts of multiple fields remain elusive. Understanding the underlying physical interactions and mechanisms for both assembly and actuation is crucial for the scientific understanding of the in- and out-of-equilibrium behaviors of colloids and their future technological applications.

This thesis focuses on exploring the impacts of combined electric and magnetic fields on the assembly and actuation of various colloidal structures from simple building blocks of spherical magnetic particles. In particular, Chapter 2 reports both experimental and computational studies on the control of orientation and actuation of linear colloidal chains by the combined biaxial magnetic field and one-dimensional AC electric field. Chapter 3 discusses the assembly of two-dimensional and pseudo-three-dimensional colloidal structures with spatial and orientational order using orthogonally applied magnetic and electric fields. Chapter 4 summarizes our key findings and proposes future directions.

References

1. Li, B.; Zhou, D.; Han, Y., Assembly and phase transitions of colloidal crystals. *Nature Reviews Materials* **2016,** *1*, 1-13.

2. Arora, A. K.; Rajagopalan, R., Applications of colloids in studies of phase transitions and patterning of surfaces. *Current opinion in colloid & interface science* **1997,** *2*, 391-396.

3. Walz, J. Y.; Sharma, A., Effect of long range interactions on the depletion force between colloidal particles. *Journal of colloid and interface science* **1994,** *168*, 485-496.

4. Ruhwandl, R.; Terentjev, E., Long-range forces and aggregation of colloid particles in a nematic liquid crystal. *Physical Review E* **1997,** *55*, 2958.

5. Yuan, Y.; Tasinkevych, M.; Smalyukh, I. I., Colloidal interactions and unusual crystallization versus de-mixing of elastic multipoles formed by gold mesoflowers. *Nature communications* **2020,** *11*, 1-14.

6. Wang, Z.; Wang, Z.; Li, J.; Tian, C.; Wang, Y., Active colloidal molecules assembled via selective and directional bonds. *Nature communications* **2020,** *11*, 1-12.

7. Colvin, V. L., From opals to optics: Colloidal photonic crystals. *Mrs Bulletin* **2001,** *26*, 637-641.

8. Takeoka, Y., Stimuli-responsive opals: colloidal crystals and colloidal amorphous arrays for use in functional structurally colored materials. *Journal of Materials Chemistry C* **2013,** *1*, 6059-6074.

9. Cersonsky, R. K.; van Anders, G.; Dodd, P. M.; Glotzer, S. C., Relevance of packing to colloidal self-assembly. *Proceedings of the National Academy of Sciences* **2018,** *115*, 1439-1444.

10. Nie, Z.; Fava, D.; Kumacheva, E.; Zou, S.; Walker, G. C.; Rubinstein, M., Self-assembly of metal–polymer analogues of amphiphilic triblock copolymers. *Nature materials* **2007,** *6*, 609-614.

11. Chen, Q.; Yan, J.; Zhang, J.; Bae, S. C.; Granick, S., Janus and multiblock colloidal particles. *Langmuir* **2012,** *28*, 13555-13561.

12. Lim, S.-H.; Lee, T.; Oh, Y.; Narayanan, T.; Sung, B. J.; Choi, S.-M., Hierarchically self-assembled hexagonal honeycomb and kagome superlattices of binary 1D colloids. *Nature Communications* **2017,** *8*, 360.

13. Berrocal, J. A.; Heideman, G. H.; de Waal, B. F. M.; Enache, M.; Havenith, R. W. A.; Stöhr, M.; Meijer, E. W.; Feringa, B. L., Engineering Long-Range Order in Supramolecular Assemblies on Surfaces: The Paramount Role of Internal Double Bonds in Discrete Long-Chain Naphthalenediimides. *Journal of the American Chemical Society* **2020,** *142*, 4070-4078.

14. Michaels, T. C. T.; Bellaiche, M. M. J.; Hagan, M. F.; Knowles, T. P. J., Kinetic constraints on self-assembly into closed supramolecular structures. *Scientific Reports* **2017,** *7*, 12295.

15. Nagarajan, R., Molecular Packing Parameter and Surfactant Self-Assembly: The Neglected Role of the Surfactant Tail. *Langmuir* **2002,** *18*, 31-38.

16. Li, F.; Josephson, D. P.; Stein, A., Colloidal assembly: the road from particles to colloidal molecules and crystals. *Angewandte Chemie International Edition* **2011,** *50*, 360-388.

17. Sun, J.; Li, Y.; Dong, H.; Zhan, P.; Tang, C.; Zhu, M.; Wang, Z., Fabrication and light-transmission properties of monolayer square symmetric colloidal crystals via controlled convective self-assembly on 1D grooves. *Advanced Materials* **2008,** *20*, 123-128.

18. Zhang, J.; Guo, J.; Mou, F.; Guan, J., Light-controlled swarming and assembly of colloidal particles. *Micromachines* **2018,** *9*, 88.

19. Huang, X.; Zhou, J.; Fu, M.; Li, B.; Wang, Y.; Zhao, Q.; Yang, Z.; Xie, Q.; Li, L., Binary colloidal crystals with a wide range of size ratios via template-assisted electric-field-induced assembly. *Langmuir* **2007,** *23*, 8695-8698.

20. Jathavedan, K.; Bhat, S. K.; Mohanty, P. S., Alternating electric-field-induced assembly of binary mixtures of soft repulsive ionic microgel colloids. *Journal of colloid and interface science* **2019,** *544*, 88-95.

21. Ma, F.; Wang, S.; Wu, D. T.; Wu, N., Electric-field–induced assembly and propulsion of chiral colloidal clusters. *Proceedings of the national academy of sciences* **2015,** *112*, 6307-6312.

22. Tang, Y.; Zhou, Y.; Zhou, D.; Chen, Y.; Xiao, Z.; Shi, J.; Liu, J.; Hong, W., Electric Field-Induced Assembly in Single-Stacking Terphenyl Junctions. *Journal of the American Chemical Society* **2020**.

23. Akella, M.; Juarez, J. J., High-throughput acoustofluidic self-assembly of colloidal crystals. *ACS omega* **2018,** *3*, 1425-1436.

24. Owens, C. E.; Shields, C. W.; Cruz, D. F.; Charbonneau, P.; López, G. P., Highly parallel acoustic assembly of microparticles into well-ordered colloidal crystallites. *Soft Matter* **2016,** *12*, 717-728.

25. Hu, M.; Butt, H.-J. r.; Landfester, K.; Bannwarth, M. B.; Wooh, S.; Thérien-Aubin, H., Shaping the Assembly of Superparamagnetic Nanoparticles. *ACS nano* **2019,** *13*, 3015-3022.

26. Wang, M.; He, L.; Yin, Y., Magnetic field guided colloidal assembly. *Materials Today* **2013,** *16*, 110-116.

27. Snezhko, A.; Aranson, I. S., Magnetic manipulation of self-assembled colloidal asters. *Nature materials* **2011,** *10*, 698-703.

28. Yang, T.; Tasci, T. O.; Neeves, K. B.; Wu, N.; Marr, D. W., Magnetic microlassos for reversible cargo capture, transport, and release. *Langmuir* **2017,** *33*, 5932-5937.

29. Patteson, A. E.; Gopinath, A.; Arratia, P. E., Active colloids in complex fluids. *Current Opinion in Colloid & Interface Science* **2016,** *21*, 86-96.

30. Zöttl, A.; Stark, H., Emergent behavior in active colloids. *Journal of Physics: Condensed Matter* **2016,** *28*, 253001.

31. Singh, D. P.; Choudhury, U.; Fischer, P.; Mark, A. G., Non-equilibrium assembly of light-activated colloidal mixtures. *Advanced Materials* **2017,** *29*, 1701328.

32. Wang, J.; Xiong, Z.; Zheng, J.; Zhan, X.; Tang, J., Light-driven micro/nanomotor for promising biomedical tools: principle, challenge, and prospect. *Accounts of chemical research* **2018,** *51*, 1957-1965.

33. Goodrich, C. P.; Brenner, M. P., Using active colloids as machines to weave and braid on the micrometer scale. *Proceedings of the National Academy of Sciences* **2017,** *114*, 257-262.

34. Adair, J. H.; Suvaci, E.; Sindel, J., Surface and Colloid Chemistry. In *Encyclopedia of Materials: Science and Technology*, Buschow, K. H. J.; Cahn, R. W.; Flemings, M. C.; Ilschner, B.; Kramer, E. J.; Mahajan, S.; Veyssière, P., Eds. Elsevier: Oxford, 2001; pp 1-10.

35. Russel, W. B.; Russel, W.; Saville, D. A.; Schowalter, W. R., *Colloidal dispersions*. Cambridge university press: 1991.

36. Parker, G., Encyclopedia of materials: science and technology. **2001**.

37. Horinek, D., DLVO Theory. In *Encyclopedia of applied electrochemistry*, Kreysa, G.; Ota, K.-i.; Savinell, R. F., Eds. Springer New York: New York, NY, 2014; pp 343-346.

38. Fritz, G.; Schädler, V.; Willenbacher, N.; Wagner, N. J., Electrosteric stabilization of colloidal dispersions. *Langmuir* **2002,** *18*, 6381-6390.

39. Semenov, A.; Shvets, A., Theory of colloid depletion stabilization by unattached and adsorbed polymers. *Soft Matter* **2015,** *11*, 8863-8878.

40. Yuan, Y., Metal nanoplatelet synthesis and dispersion in suspension: Silver, copper, nickel and related alloys. **2007**.

41. Alidoosti, E.; Zhao, H., On the impact of electrostatic correlations on the double-layer polarization of a spherical particle in an alternating current field. *Langmuir* **2018,** *34*, 5592-5599.

42. Green, N. G.; Morgan, H., Dielectrophoresis of submicrometer latex Spheres. 1. Experimental results. *The Journal of Physical Chemistry B* **1999,** *103*, 41-50.

43. O'Konski, C. T., Electric properties of macromolecules.v. theory of ionic polarisation in polyelectrolytes. *The Journal of Physical Chemistry* **1960,** *64*, 605-619.

44. Ma, F.; Yang, X.; Wu, N., Directed assembly of anisotropic particles under external fields. In *Anisotropic Particle Assemblies*, Elsevier: 2018; pp 131-165.

45. Grosse, C.; Shilov, V. N., Theory of the low-frequency electrorotation of polystyrene particles in electrolyte solution. *The Journal of Physical Chemistry* **1996,** *100*, 1771-1778.

46. Klapp, S. H., Collective dynamics of dipolar and multipolar colloids: From passive to active systems. *Current opinion in colloid & interface science* **2016,** *21*, 76-85.

47. Beltramo, P. J.; Furst, E. M., Predicting the disorder–order transition of dielectrophoretic colloidal assembly with dielectric spectroscopy. *Electrophoresis* **2013,** *34*, 1000-1007.

48. Zhou, H.; Preston, M. A.; Tilton, R. D.; White, L. R., Calculation of the electric polarizability of a charged spherical dielectric particle by the theory of colloidal electrokinetics. *Journal of colloid and interface science* **2005,** *285*, 845-856.

49. Yang, X.; Johnson, S.; Wu, N., The Impact of Stern-Layer Conductivity on the Electrohydrodynamic Flow Around Colloidal Motors under an Alternating Current Electric Field. *Advanced Intelligent Systems* **2019,** *1*, 1900096.

50. Du, D.; Biswal, S. L., Micro-mutual-dipolar model for rapid calculation of forces between paramagnetic colloids. *Physical Review E* **2014,** *90*, 033310.

51. Reuss, F. F., Sur un nouvel effet de l'électricité galvanique. *Mem. Soc. Imp. Natur. Moscou* **1809,** *2*, 327-337.

52. Bazant, M. Z.; Squires, T. M., Induced-charge electrokinetic phenomena. *Current Opinion in Colloid & Interface Science* **2010,** *15*, 203-213.

53. Prieve, D. C.; Sides, P. J.; Wirth, C. L., 2-D assembly of colloidal particles on a planar electrode. *Current Opinion in Colloid & Interface Science* **2010,** *15*, 160-174.

54. Fagan, J. A.; Sides, P. J.; Prieve, D. C., Vertical oscillatory motion of a single colloidal particle adjacent to an electrode in an AC electric field. *Langmuir* **2002,** *18*, 7810-7820.

55. Böhmer, M., In situ observation of 2-dimensional clustering during electrophoretic deposition. *Langmuir* **1996,** *12*, 5747-5750.

56. Ma, F.; Yang, X.; Zhao, H.; Wu, N., Inducing propulsion of colloidal dimers by breaking the symmetry in electrohydrodynamic flow. *Physical review letters* **2015,** *115*, 208302.

57. Ristenpart, W.; Aksay, I. A.; Saville, D., Electrically guided assembly of planar superlattices in binary colloidal suspensions. *Physical review letters* **2003,** *90*, 128303.

58. Ma, F. Electric-field assembly of colloids with anisotropic interactions. Colorado School of Mines, 2015.

59. Saville, D., Electrohydrodynamics: the Taylor-Melcher leaky dielectric model. *Annual review of fluid mechanics* **1997,** *29*, 27-64.

60. Haque, M. A. Corona Induced Electrohydrodynamics: A Contactless Method to Manipulate Liquids. University of Toledo, 2019.

61. Mozumder, A., Effect of an external electric field on the yield of free ions. I General results from the Onsager theory. *The Journal of Chemical Physics* **1974,** *60*, 4300-4304.

62. Ryu, J. C.; Park, H. J.; Park, J. K.; Kang, K. H., New electrohydrodynamic flow caused by the Onsager effect. *Physical review letters* **2010,** *104*, 104502.

63. Bowles, S. E.; Wu, W.; Kowalewski, T.; Schalnat, M. C.; Davis, R. J.; Pemberton, J. E.; Shim, I.; Korth, B. D.; Pyun, J., Magnetic assembly and pyrolysis of functional ferromagnetic colloids into one-dimensional carbon nanostructures. *Journal of the American Chemical Society* **2007,** *129*, 8694-8695.

64. Gong, J.; Wu, N., Electric-field assisted assembly of colloidal particles into ordered nonclose-packed arrays. *Langmuir* **2017,** *33*, 5769-5776.

65. Straube, A. V.; Dullens, R. P.; Schimansky-Geier, L.; Louis, A. A., Zigzag transitions and nonequilibrium pattern formation in colloidal chains. *The Journal of chemical physics* **2013,** *139*, 134908.

66. Li, Z.; Yang, F.; Yin, Y., Smart materials by nanoscale magnetic assembly. *Advanced Functional Materials* **2020,** *30*, 1903467.

67. Yakovlev, E. V.; Komarov, K. A.; Zaytsev, K. I.; Kryuchkov, N. P.; Koshelev, K. I.; Zotov, A. K.; Shelestov, D. A.; Tolstoguzov, V. L.; Kurlov, V. N.; Ivlev, A. V., Tunable two-dimensional assembly of colloidal particles in rotating electric fields. *Scientific reports* **2017,** *7*, 1-10.

68. Melle, S.; Calderón, O. G.; Rubio, M. A.; Fuller, G. G., Rotational dynamics in dipolar colloidal suspensions: video microscopy experiments and simulations results. *Journal of Non-Newtonian Fluid Mechanics* **2002,** *102*, 135-148.

69. Martin, J. E.; Anderson, R. A.; Williamson, R. L., Generating strange magnetic and dielectric interactions: Classical molecules and particle foams. *The Journal of chemical physics* **2003,** *118*, 1557-1570.

70. Bharti, B.; Kogler, F.; Hall, C. K.; Klapp, S. H.; Velev, O. D., Multidirectional colloidal assembly in concurrent electric and magnetic fields. *Soft Matter* **2016,** *12*, 7747-7758.

71. Demirörs, A. F.; Courty, D.; Libanori, R.; Studart, A. R., Periodically microstructured composite films made by electric-and magnetic-directed colloidal assembly. *Proceedings of the National Academy of Sciences* **2016,** *113*, 4623-4628.

72. Martin, J. E.; Snezhko, A., Driving self-assembly and emergent dynamics in colloidal suspensions by time-dependent magnetic fields. *Reports on Progress in Physics* **2013,** *76*, 126601.

73. Erb, R. M.; Son, H. S.; Samanta, B.; Rotello, V. M.; Yellen, B. B., Magnetic assembly of colloidal superstructures with multipole symmetry. *Nature* **2009,** *457*, 999-1002.

74. Hu, L.; Zhang, R.; Chen, Q., Synthesis and assembly of nanomaterials under magnetic fields. *Nanoscale* **2014,** *6*, 14064-14105.

75. Skjeltorp, A. T., One-and two-dimensional crystallization of magnetic holes. *Physical Review Letters* **1983,** *51*, 2306.

76. Shemi, O.; Solomon, M. J., Self-Propulsion and Active Motion of Janus Ellipsoids. *The Journal of Physical Chemistry B* **2018,** *122*, 10247-10255.

77. Samin, S.; van Roij, R., Self-propulsion mechanism of active Janus particles in near-critical binary mixtures. *Physical review letters* **2015,** *115*, 188305.

78. Wang, W.; Lv, X.; Moran, J. L.; Duan, S.; Zhou, C., A practical guide to active colloids: choosing synthetic model systems for soft matter physics research. *Soft matter* **2020,** *16*, 3846-3868.

79. Straube, A. V.; Tierno, P., Tunable interactions between paramagnetic colloidal particles driven in a modulated ratchet potential. *Soft Matter* **2014,** *10*, 3915-3925.

80. Aranson, I. S., Active colloids. *Physics-Uspekhi* **2013,** *56*, 79.

81. Li, G.-J.; Karimi, A.; Ardekani, A. M., Effect of solid boundaries on swimming dynamics of microorganisms in a viscoelastic fluid. *Rheologica acta* **2014,** *53*, 911-926.

82. Lumay, G.; Obara, N.; Weyer, F.; Vandewalle, N., Self-assembled magnetocapillary swimmers. *Soft Matter* **2013,** *9*, 2420-2425.

83. Nishiguchi, D.; Sano, M., Mesoscopic turbulence and local order in Janus particles self-propelling under an ac electric field. *Physical Review E* **2015,** *92*, 052309.

84. Ikeda, K.; Kim, K., Lane formation dynamics of oppositely self-driven binary particles: effects of density and finite system size. *Journal of the Physical Society of Japan* **2017,** *86*, 044004.

85. Rex, M.; Royall, C. P.; van Blaaderen, A.; Löwen, H., Lane formation in driven colloidal mixtures: is it continuous or discontinuous? *arXiv preprint arXiv:0812.0908* **2008**.

86. Ikeda, M.; Wada, H.; Hayakawa, H., Instabilities and turbulence-like dynamics in an oppositely driven binary particle mixture. *EPL (Europhysics Letters)* **2012,** *99*, 68005.

87. Wensink, H.; Löwen, H., Emergent states in dense systems of active rods: from swarming to turbulence. *Journal of Physics: Condensed Matter* **2012,** *24*, 464130.

CHAPTER 2

ASSEMBLY AND PROPULSION OF LINEAR COLLOIDAL CHAINS UNDER COMBINED ELECTRIC AND MAGNETIC FIELDS

2.1 Abstract

The fascinating efficiency and dynamics of micromachines in bacteria cells have inspired the scientific community to search for artificial microrobots for applications in chemical sensing, cargo transport, and waste remediation. While much work has been focused on exploring new self-propulsion mechanisms, recent trends have shifted towards guided locomotion under external fields. Here, we report a strategy combining a planar magnetic field with a one-dimensional electric field to assemble and actuate linear chains made of paramagnetic microspheres. While a horizontal chain lying on the substrate is symmetric fore and aft and does not translate, a two-dimensional magnetic field can tilt the chain with an angle relative to the substrate. A superimposed alternating-current (AC) electric field leads to the propulsion of tilted chains along the substrate. Our numerical simulation and experiments confirm that the electrohydrodynamic flow along the electrode is unbalanced surrounding the tilted chain, generating hydrodynamic stresses that both propel the chain and reorient it slightly towards the substrate. Our work takes advantage of both fields where the magnetic field controls chain orientation while the electric field provides power for locomotion. Without the necessity to synthesize complex-shaped micromotors with intricate building blocks, our work reveals a propulsion mechanism that breaks the symmetry of hydrodynamic flow by manipulating the orientation of a microscopic object.

2.2 Introduction

The unifying idea of locomotion for a microscopic object in a low Reynolds number regime[1] is to break its geometric or surface asymmetry, create time-asymmetry in actuation, or couple the motion with non-Newtonian fluid rheology. Among these, body deformation and shape morphing have appeared to be an efficient scheme adopted by biological motors. For example, the corkscrew rotation of bacteria flagella and tail-whipping of sperms demonstrate various kinds of undulatory morphological changes that allow microorganisms to move in three dimensions.[2] On the other hand, most synthetic micro-swimmers have rigid bodies. One often resorts to breaking the symmetry of geometric shapes and/or interfacial properties for locomotion. Classic examples include the motion of bi-metallic or metallodielectric Janus particles due to self-diffusiophoresis,[3-4] self-electrophoresis,[5] induced-charge electroosmosis,[6] light-induced self-thermophoresis,[7] and bubble recoil.[8-9] Irrespective of their underlying swimming mechanisms, the much-needed phoretic force has to be induced via either asymmetric surface functionalization or geometric design.[10-15] Although some recent studies have reported the fabrication of shape-adaptable microbots,[16-18] they often require advanced manufacturing processes that typically suffer from scalability.

While self-propelled micromachines offer excellent opportunities to study the physics of active matter out of equilibrium, they are often limited by the lack of directionality or toxic fuels.[19-22] On the contrary, external sources such as electric field, magnetic field, acoustic field, or optical field can provide better control in both speed and propulsion direction.[23-33] Inspired by the versatility of multiaxial magnetic fields and rich nonlinear electrokinetic phenomena under alternating-current (AC) electric fields, in this work, we show how the combined fields can actuate

linear chains assembled from magnetic microspheres and subsequently control their propulsion speed and direction by tuning their relative orientation to the substrate.

2.3 Experimental Methods

Materials. Dynabeads® MyOne™ Carboxylic Acid (1 μm magnetic latex microspheres) were purchased from Thermo Fisher Scientific (Waltham, MA). They were cleaned four times in deionized (DI) water via centrifugation before redispersing in deionized (DI) water. Indium tin oxide (ITO) glass slides (15-25 Ω per sq) were purchased from Sigma-Aldrich. Poly(sodium 4-styrene sulfonate) (molecular weight = 70,000) was purchased from Sigma-Aldrich.

Experimental Setup. As shown in Figure 2.1, we used two ITO glass slides as the bottom and top electrodes. They were separated by a 100-μm thick non-conducting polyester film as spacers, forming a chamber in which 5-10 μL of dilute Dynabeads® was added. To prevent particle adhesion to the ITO substrates, we cleaned the substrate with acetone and isopropanol for 15 minutes inside an ultrasonic chamber. We then exposed the ITO glass slides to oxygen plasma for 1 minute. Finally, we coated them with aqueous poly (sodium 4-styrene sulfonate) solution (5 mg/mL). The coating helps prevent adhesion of the negatively charged Dynabeads® onto the substrates. An AC electric field was applied perpendicularly between two ITO glasses via a function generator (RIGOL DS1054Z). The range of the voltage applied is 0-20 volts peak-to-peak and frequency, f_E, is between 500 and 50,000 Hz. Three-dimensional (3D) magnetic fields were generated with five air-cored copper solenoid coils of 50 mm inner diameter, 51 mm length, and 400 turns with a current capacity of 3.5A. Four of the coils were arranged orthogonally in the *x-y* plane, and the fifth coil was placed directly on top of the ITO electrode along the *z*-direction.

Using a custom-made MATLAB program, we can apply 3D magnetic fields with variable strength, frequency, and phase angle conveniently.

Image analysis. To observe and record the dynamics of colloidal particles, an inverted optical microscope (Olympus IX71) was used with a Silicon Video 642 high-speed black/white camera to capture the particles' motion in 30 frames per second. We used ImageJ[34] to analyze the high-speed videos, from which the chain length and velocities of chains with different tilting angles were obtained.

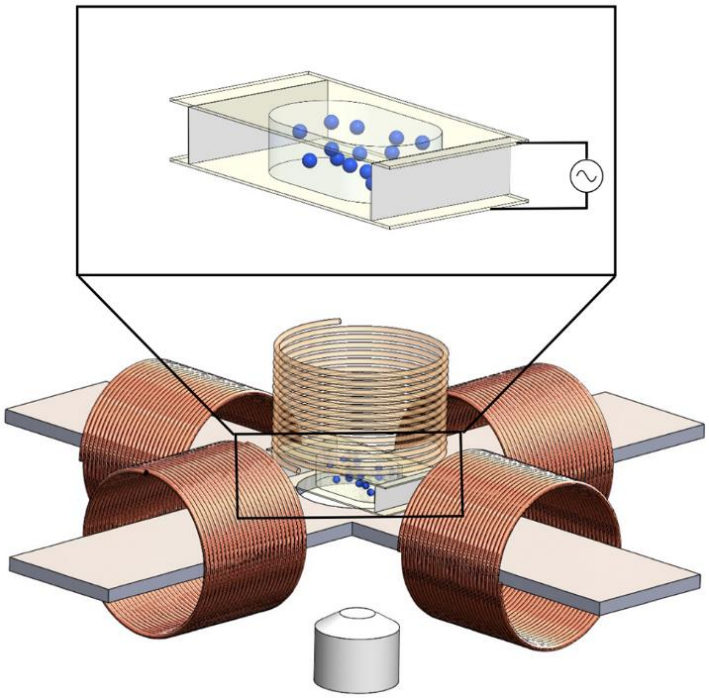

Figure 2.1 Schematic of the experimental setup using combined electric (in the z-direction) and magnetic fields (in x-, y-, and z-directions). The range of the applied electric field is 2-20 volts peak-to-peak (Vpp) across a 100 μm gap and 500-50,000 Hz. And the range of the applied magnetic field is 0 -16 mT and 20-60 Hz.

2.4 Results and Discussion

We first assembled 1 μm magnetic microspheres into linear colloidal chains of different lengths (Figure 2a) along the *y*-direction by applying a 1D magnetic field along the *y*-direction, i.e. $\mathbf{B} = B_y \cos(\omega_M t)\hat{\mathbf{y}}$, where $\omega_M = 2\pi f_{\mathrm{M}}$ is the angular frequency of the magnetic field. Intuitively, the chain formation is caused by the attraction between induced magnetic dipoles on each particle. When we superimposed an additional magnetic field along the *z*-direction, i.e. $B_z \cos(\omega_M t)\hat{\mathbf{z}}$, we can see that the assembled chains were tilted with respect to the substrate (Figure 2.2b). By measuring the projection length of a tilted chain, we can determine the chain tilting angle, θ_c, which is

the angle between its long axis and $\hat{\mathbf{z}}$. Zero θ_c corresponds to a vertical chain normal to the substrate, and the chain is horizontal and lying on the substrate when $\theta_c = 90°$. It can be seen in Figure 2.2c that the chain orientation is primarily controlled by the ratio of field strength $B_{\mathrm{y}} / B_{\mathrm{z}}$. Although chain lengths vary, θ_c is approximately equal to $\theta_{\mathrm{M}} = \tan^{-1}\left(B_{\mathrm{y}} / B_{\mathrm{z}}\right)$, i.e., the magnetic field angle. We noticed that none of the tilted chains translated. Unlike electrostatic charges, there is no magnetic monopoles. Therefore, magnetophoresis only occurs when there is a field gradient. Since the fields applied here are uniform in space, the assembled chains do not translate.

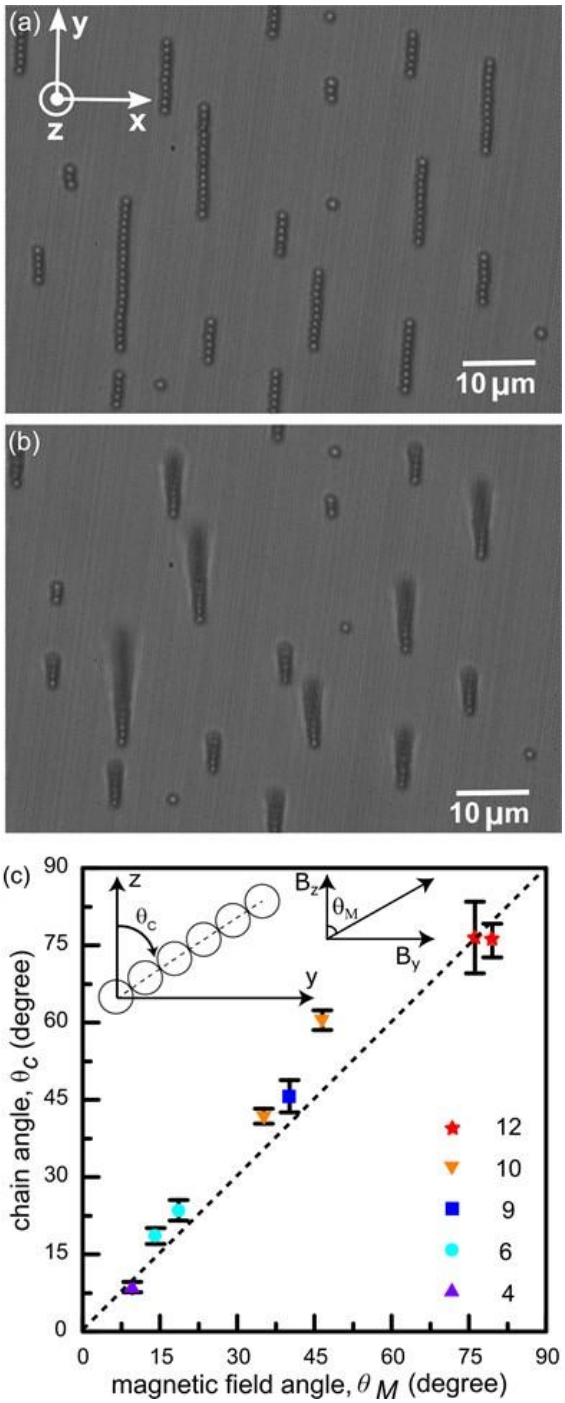

Figure 2.2 Tilted colloidal chains under a 2D magnetic field only. (a) An optical image of horizontal colloidal chains under 1D magnetic field ($B_y = 4.25$ mT). (b) An optical image of the tilted chains of different lengths ($B_y = 4.25$ mT and $B_z = 6$ mT). The chain tiling angle $\theta_C = 40 \pm 6°$. (c) The chain angle θ_C as a function of the magnetic field angle θ_M for different chain lengths. The legends indicate the number of monomers along a single chain.

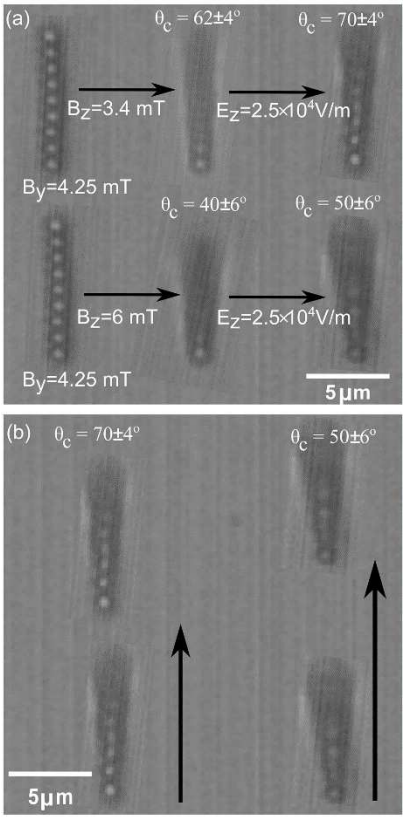

Figure 2.3 Tilting and translation of colloidal chains under combined electric and magnetic fields. (a) Tilting of a nonamer chain under different magnetic and electric fields (E_z = 2.5×10^4 V/m and f_E = 1,300 Hz). (b) The nonamer with different tilting angles translates at different speeds (in an eight-second interval).

Interestingly, we observed two new phenomena when we superimposed an additional AC electric field along the *z*-axis, i.e. $\mathbf{E} = E_z \cos(\omega_E t)\hat{\mathbf{z}}$, where $\omega_E = 2\pi f_E$ is the electric field angular frequency and E_z is the field strength. First, we found that the chain angle θ_C increases, i.e., the chains tilted more towards the substrate. This effect can be seen clearly in Figure 2.3a, where the chain projection length becomes larger when the electric field is on. Secondly, the titled chains started to translate along the positive *y*-direction on the substrate (Figure 2.3b). Interestingly, the chain propulsion speed depends on its tilting angle. As shown in Figure 2.4, when θ_c is 0° or 90°, i.e., for a perfectly vertical or horizontal chain, its translation speed is zero. The speed, however, varies non-monotonically when $0° < \theta_c < 90°$ and reaches the maximum when θ_c is ~ 45°. The

relatively small error bars in velocity also indicate that it is a weak function on chain length. In the following, we will investigate both phenomena in detail.

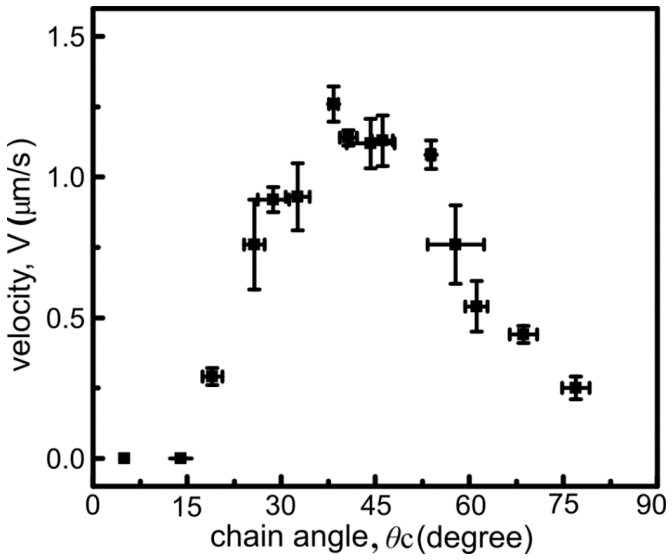

Figure 2.4 The propulsion speed of tilted chains as a function of the chain angle. Error bars indicate the variance of change length from 4 to 14.

The fact that θ_C increases when an electric field is superimposed in the *z*-direction is counterintuitive as the additional attraction between induced electric dipoles should align the chain closer to the *z*-axis. To understand why we theoretically model the energy of a linear chain under combined fields by assuming that both magnetic ($\mathbf{m}_i^M$) and electric dipole moments ($\mathbf{m}_i^E$) in each particle are:

$$\mathbf{m}_i^M = \chi V\mathbf{B} = \frac{4\pi R^3 \chi \mu_s \mathbf{H}}{3} = \frac{4\pi\mu_s R^3\left(\mu_p - \mu_s\right)\mathbf{H}}{\mu_p + 2\mu_s}, \qquad (2.1)$$
$$\mathbf{m}_i^E = 4\pi\varepsilon_0\varepsilon_s R^3 K\mathbf{E}$$

where χ is the particle volume susceptibility, μ_p (μ_s) is the permeability of the particle (solvent), *H* is the magnetic field strength, *R* is the particle radius, ε_s is the solvent dielectric constant, ε_0 is the vacuum permittivity, and K is the electric polarization coefficient,[35-36] which depends on the

electric field frequency f_{E}, Debye length κ^{-1}, particle zeta potential ζ_{p}, particle radius R, and electrical properties such as conductivity and dielectric constant of both particle and solvent. If we assume that the magnetic (electric) dipoles are aligned with the external magnetic (electric) field direction, the total energy of a colloidal chain can be expressed as a sum of both dipolar interaction between two particles[37-38] and the gravitational energy:

$$U = \sum_{i=1}^{N-1}\sum_{j>i}^{N}\left\{\frac{A_{\mathrm{M}}}{r_{\mathrm{ij}}^{3}}\left[1-3\cos^{2}\left(\theta_{\mathrm{C}}-\theta_{\mathrm{M}}\right)\right]+\frac{A_{\mathrm{E}}}{r_{\mathrm{ij}}^{3}}\left(1-3\cos^{2}\theta_{\mathrm{C}}\right)\right\} + \sum_{i=1}^{N}\frac{4\pi R^{4} g\left(\rho_{\mathrm{p}}-\rho_{\mathrm{s}}\right)\left[2\left(i-1\right)\cos\theta_{C}+1\right]}{3}, \tag{2.2}$$

where $A_{\mathrm{M}} = 4\pi\mu_{\mathrm{s}}R^{6}H^{2}\left(\mu_{\mathrm{p}}-\mu_{\mathrm{s}}\right)^{2}/\left(\mu_{\mathrm{p}}+2\mu_{\mathrm{s}}\right)^{2}$, $A_{\mathrm{E}} = 4\pi\varepsilon_{0}\varepsilon_{\mathrm{s}}R^{6}K^{2}E_{\mathrm{z}}^{2}$, $H = \sqrt{H_{\mathrm{y}}^{2}+H_{\mathrm{z}}^{2}}$, ρ_{p} (ρ_{s}) is the particle (solvent) density, and r_{ij} is the center-to-center separation between particles *i* and *j*.

In Figure 2.5a, we plot the magnetic energy, magnetic and gravitational energy, and the magnetic, electric, and gravitational energy of a decamer chain with different tilting angles under the same field condition. The minimum in each curve corresponds to the equilibrium chain angle θ_c under each energetic consideration. With an applied magnetic field, the gravitational force tends to tilt the chain towards the substrate, while the electric field reorients the chain towards the *z*-direction, making θ_c smaller. The impact of the electric field on chain orientation can be seen more clearly in Figure 2.5b. Our experimental measurement for chain angles under magnetic field only (blue squares) matches well with the theoretical prediction, i.e., $\theta_c \approx \theta_M$. On the other hand, the chain angles (red squares) shift towards the opposite direction under combined electric and magnetic fields compared to the theory (indicated by the red dashed line).

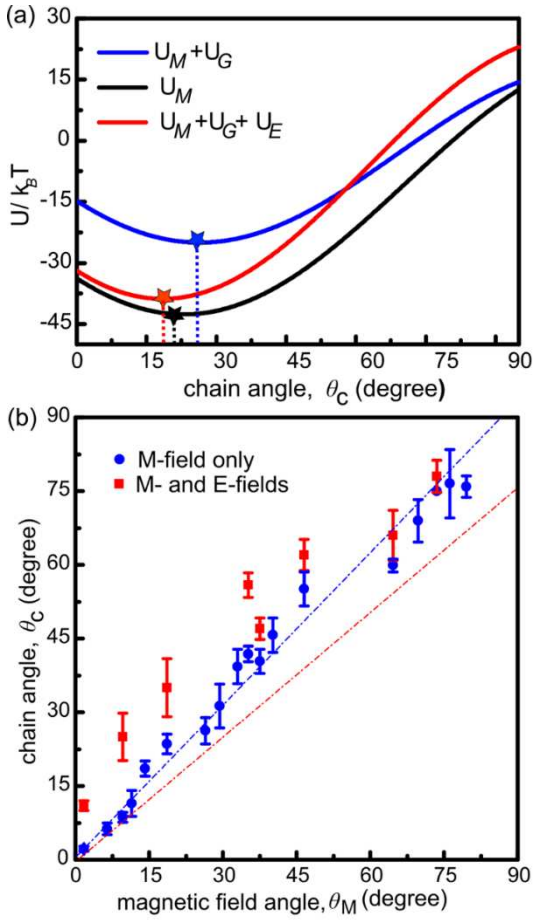

Figure 2.5 The impact of magnetic, electric, and gravitational fields on the tilting angle of colloidal chains. (a) The calculated energy of a decamer with different tilting angles under the same field condition. B_y = 2.2 mT, B_z = 5.3 mT, f_M = 50 Hz, $E_z = 2.5\times10^4$ V/m, and f_E = 1300 Hz. Symbols represent the minima in each curve. (b) The tilting angle of a decamer under magnetic field only and combined magnetic and electric fields. B_y = 3.4 mT, and B_z varies from 0.5 to 15.5 mT. $E_z = 2.5\times10^4$ V/m, and f_E = 1300 Hz. The dashed lines are theoretical predictions, and squares are experimental measurements.

The discrepancy between experiments and theory in chain orientation and the fact that chains started to translate clearly indicate that the applied electric field introduces additional effects beyond inducing dipolar interactions between neighboring monomers. Indeed, it is known that an electrohydrodynamic (EHD) flow[39] can be generated surrounding a dielectric microsphere when it is adjacent to a conducting substrate and is subject to a low-frequency AC electric field (f_E < 10

kHz). The applied AC electric field polarizes the conducting substrate and induces excess mobile ions in the diffusive layer. In the meantime, the same electric field also polarizes the nearby particle (and its associated diffusive layer) and generates an induced dipole. The dipole itself induces an electric field, whose tangential component along the substrate drives the electroosmotic flow on both mobile ions and solvent. Because the applied field is responsible for generating both induced charges in the diffusive layer and the tangential polarization field near the electrode, the EHD flow is a nonlinear electrokinetic phenomenon. Both experiments and theory have confirmed that the flow velocity is proportional to the applied electric field strength squared and inversely proportional to frequency.[40-41]

More interestingly, depending on the particle's effective dipole, the EHD flow can be extensile or contractile, i.e., directed away or towards the particle. For a spherical particle, its surrounding EHD flow is symmetric. Although the particle itself does not move, its neighboring particles can be attracted or repelled due to the electrohydrodynamic interaction. On the other hand, a net EHD flow ensues around an asymmetric particle such as colloidal dimers with different diameters, zeta potentials, or chemical compositions on the two lobes.[42] Herein, although a horizontal chain is symmetric fore and aft, the symmetry will be broken once it is tilted. Therefore, it is plausible that an unbalanced EHD flow is induced surrounding a tilted chain which causes its propulsion. Our experimental observation that a vertical or horizontal chain does not translate supports this idea since the EHD flow will be symmetric in both situations. Moreover, if the EHD flow is extensile, i.e., directed away from the chain, it will generate a hydrodynamic attraction between the chain and the substrate, which can further tilt the chain towards the substrate. Therefore, we hypothesize that an extensile electrohydrodynamic (EHD) flow is also generated under the AC electric field, which not only reorients the chain towards the substrate and but propels

it towards the positive *y*-direction. To quantitatively test our hypothesis, we resort to numerical simulations by using COMSOL Multiphysics® in the following.

2.5 Numerical Simulation

Since a full 3D simulation of the colloidal chains will be computationally expensive, we focused on 2D calculations. To validate our method, we first model the electric potential and EHD flow surrounding a R = 1 μm magnetic microsphere near a conducting electrode that is grounded (Figure 2.6). The top electrode (not shown) is separated from the bottom one by $2H$ = 100 μm. We assume that the Debye length κ^{-1} (~ 100 nm) is much smaller than the particle radius, i.e., $\kappa R \gg 1$, and both Peclet ($\mathrm{Pe} = uR/D \sim 10^{-3}$, where u is fluid velocity and D is the ion diffusivity) and Reynolds numbers ($\mathrm{Re} = \rho u R/\mu \sim 10^{-6}$, where ρ and μ are particle density and solvent viscosity, respectively.) are small. Consequently, the Gauss's equation governing the electric potential and Stokes equations governing the fluid flow can be simplified and decoupled within the thin double layer approximation:

$$\nabla^2 \psi = 0, \tag{2.3}$$

$$\nabla \cdot \mathbf{u} = 0, \text{ and} \tag{2.4}$$

$$-\nabla P + \nabla^2 \mathbf{u} = 0, \tag{2.5}$$

where $\psi e^{-i\omega_E t}$, P, and $\mathbf{u}$ denote the electric potential, fluid pressure, and fluid velocity beyond the double layer, respectively.

The boundary conditions for solving the electric potential ψ are listed in the following. (i) Far away from both particle and electrode (boundaries 2, 3, and 4), the potential is equal to the applied electric potential

$$z \to \infty, \qquad \psi = -E_\infty z, \tag{2.6}$$

where $E_\infty = \frac{\psi_0}{2H}\left(1 - \frac{\kappa D}{\omega_E H}\right)$ and $\psi_0 e^{-i\omega t}$ is the applied electric potential between two electrodes.[39]

(ii) The diffusive layer (boundary 1) near the electrode acts as a capacitor in the thin-double-layer approximation.[43] A balance of currents leads to

$$-i\omega_E \psi = \frac{\sigma_m}{\varepsilon \varepsilon_0 \kappa} \hat{\mathbf{z}} \cdot \nabla \psi, \tag{2.7}$$

where $i = \sqrt{-1}$, ε_0 is the vacuum permittivity, ε is the particle's dielectric constant, and σ_m is the real conductivity of the medium.

(iii) On the particle surface (boundary 5), a current balance applied to a slab-shaped control volume yields

$$\nabla \psi \cdot \hat{\mathbf{n}}_\mathbf{s} = -\lambda \nabla_s^2 \psi, \tag{2.8}$$

where $\nabla_s^2 \psi = \nabla_s \cdot \nabla_s \psi$ is the surface Laplacian[44] and $\hat{\mathbf{n}}_\mathbf{s}$ is the unit normal vector of the particle surface. λ is defined as the ratio of the surface conductivity of the particle and the (complex) conductivity of the medium:[39, 45]

$$\lambda = \frac{\sigma_p^s}{\sigma_m - \mathrm{i}\,\varepsilon_m \varepsilon_0 \omega_E} = \frac{\sigma_p^{s,d} + \sigma_p^{s,i}}{\sigma_m - \mathrm{i}\,\varepsilon_m \varepsilon_0 \omega_E}, \tag{2.9}$$

where $\sigma_p^{s,d}$ is the diffusive-layer surface conductivity and $\sigma_p^{s,i}$ is the Stern-layer conductivity.[45] λ is also related to the polarization coefficient *K* of the particle via the following relationship

$$\lambda = \frac{1 + 2K}{2 - 2K}. \tag{2.10}$$

It should be noted that our simulation equations are similar to what has been proposed by Ristenpart et al.,[39] except for one noticeable difference in the boundary condition of Eq. (2.7). Instead of an *ad hoc* assumption of zero electric field normal to the substrate, we take Yariv and Schnitzer's systematic approach[43] in deriving the correct boundary condition on the electrode.

After solving the electric potential ψ, we can then solve the Stokes Eqs. (4) and (5) with the following boundary conditions for fluid velocity.

(i) Electroosmotic slip on the electrode right outside of the diffusive layer (boundary 1),

$$\begin{aligned} \mathbf{u}\cdot\hat{\mathbf{x}} &= -\frac{\varepsilon\varepsilon_0}{\mu}\cdot\left\langle \nabla_t\psi\cdot\psi\right\rangle = -\frac{\varepsilon\varepsilon_0}{2\mu}\cdot \mathrm{Re}\left(\nabla_t\psi\cdot\psi^*\right), \\ \mathbf{u}\cdot\hat{\mathbf{z}} &= 0 \end{aligned} \tag{2.11}$$

where ∇_t is the tangential gradient along the electrode, $\langle\cdot\rangle$ represents time-average a quantity, Re(·) is the real part of a complex number, and * indicates the complex conjugate.

(ii) No slip on the particle surface (boundary 5),

$$\mathbf{u} = 0\,. \tag{2.12}$$

(iii) Far away from both particle electrode (boundaries 2, 3, and 4),

$$\mathbf{u} = 0 \quad \text{and} \quad P = 0\,. \tag{2.13}$$

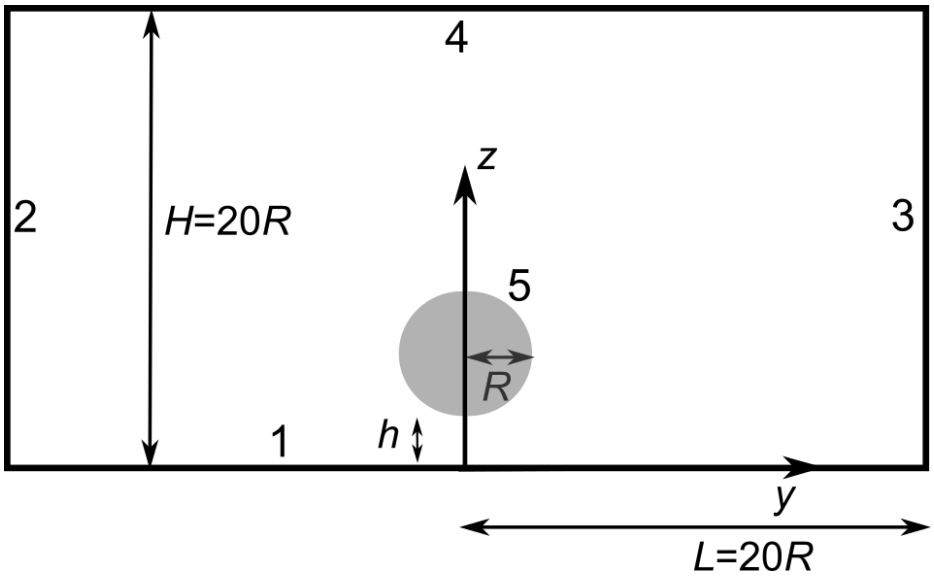

Figure 2.6 The two-dimensional computational box that models the electric potential and EHD flow around a microsphere near a grounded conducting substrate (located at z = 0). The box size is 40R by 20R, where R is the particle radius.

Table 2.1 Typical parameters used in COMSOL simulation.

Parameter	Symbol	Value	Unit
Angular frequency	ω_E	8168	rad/s
Applied potential (peak)	ψ_0	5	V
Debye layer thickness[a]	κ^{-1}	100	nm
Diffusive-layer (particle) surface conductivity[b]	$\sigma_p^{s,d}$	46.3	pS
Electrode separation	$2H$	100	μm
Ion diffusivity	D	2×10^{-9}	m^2/s
Medium conductivity[b]	σ_m	1.5×10^{-4}	S/m
Particle density[c]	ρ	1.8×10^{3}	kg/m^3
Particle dielectric constant[46]	ε_p	2.4	-
Particle radius	R	0.5	μm
Particle-substrate separation[d]	h	900	nm
Stern-layer (particle) surface conductivity	$\sigma_p^{s,i}$	200	pS
Temperature	T	298	K
Viscosity	μ	10^{-3}	Pa·s
Zeta potential[e]	ζ	-60	mV

[a]While we used deionized water, dissolved carbon dioxide and ion leaching from the substrate make a Debye length of ~100 nm more realistic.

[b]Calculated based on ref. [45].
[c]Information provided by the vendor.
[d]Calculated based on the balance of double-layer repulsion and gravitational force.
[e]Measured.

We list all parameters needed for numerical computation in Table 2.1. The results for both electric potential and flow field surrounding a 1 μm microsphere are shown in Figure 2.7. The separation between the particle and substrate, h ~ 900 nm, is determined by balancing their double-layer repulsion, van der Waals attraction, and buoyancy force. For Dynabeads® particles, their measured zeta potential is $\zeta = -60 \pm 4°$. With an additional Stern-layer conductivity estimated from latex particles,[45] its effective surface conductivity (the sum of diffusive-layer and Stern-layer conductivities) can be higher than the medium conductivity, i.e., the Dukhin number $\mathrm{Du} = \sigma_p^s / \sigma_m R > 1$. As a result, the particle has a positive induced dipole (Re(K) > 0) under the AC electric field. Therefore, the equipotential lines shown in Figure 2.7a are tangential to the particle. Moreover, the electric potential along the electrode (just outside of the double layer) becomes more negative away from the particle. Consequently, the potential gradient is negative, i.e., directed towards the particles. We emphasize that although the electrode itself is equipotential as a conducting substrate, $\psi(z=0)$ here is the potential just outside of the Debye layer. In comparison, if the particle zeta potential is low, e.g., $\zeta = -20°$, it will be negatively polarized. As shown in Figure 2.7c, the equipotential lines are perpendicular to the particle, and the potential gradient along the electrode is directed away from the particle. The electric potential calculated from Eq. (2.3) dictates the slip velocity along the electrode through the boundary condition in Eq. (2.11). Figures 2.7b shows the extensile hydrodynamic flow, i.e., the counterclockwise EHD flow directed away from the positively polarized particle. In contrast, the flow is contractile or directed towards the particle for a negatively polarized particle (Figure 2.7d). Note that the EHD flow is

symmetric around the microsphere. Therefore, the particle itself will not translate along the substrate. These results are consistent with previous experiments and simulations.[39, 45]

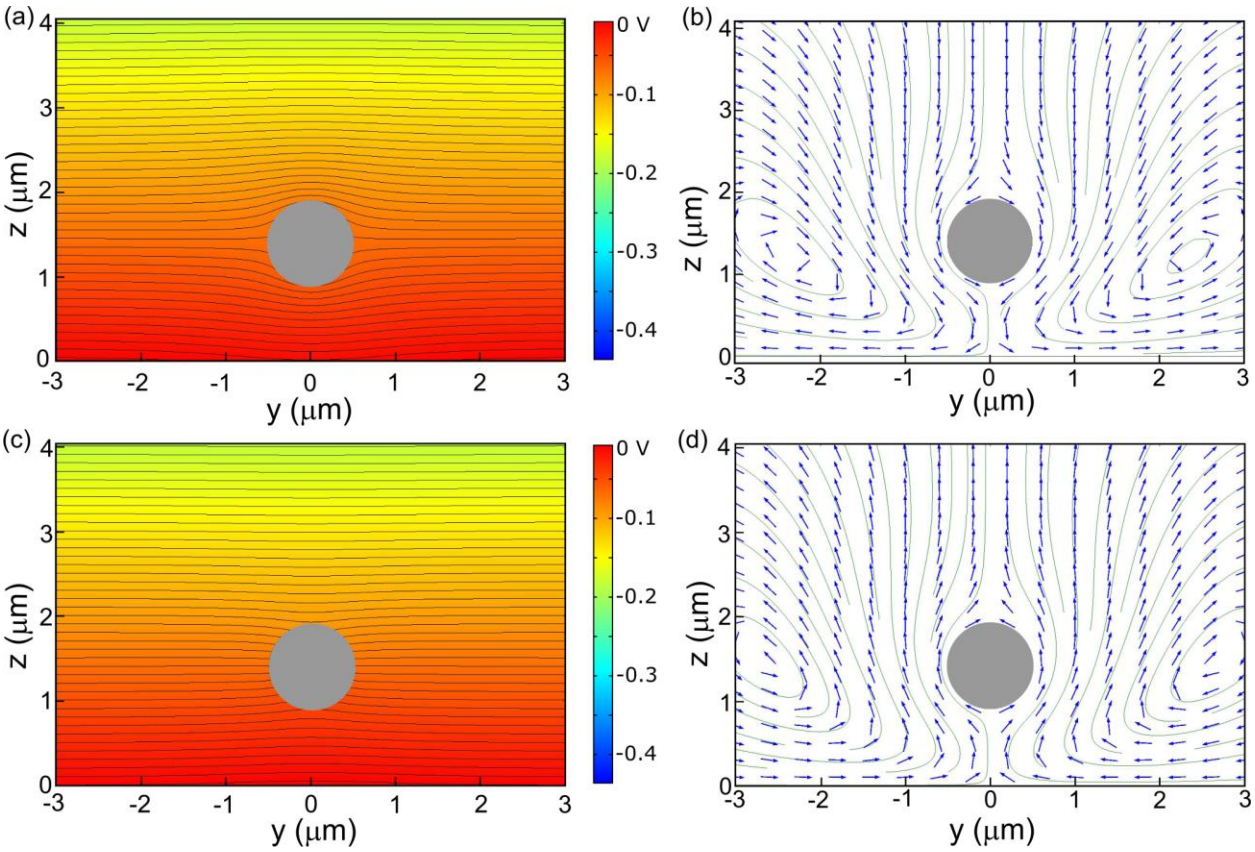

Figure 2.7 The real part of electric potential, Re(ψ), and the streamlines of the EHD flow around a 1 μm magnetic microsphere near an electrode. The particle is separated from the electrode with h = 0.9 μm. (a) and (b): ζ = -60 mV. (c) and (d): ζ = -20 mV. All other parameters are listed in Table 2.1.

We performed experiments to test whether the EHD flow surrounding the 1 μm Dynabeads® is extensile or contractile. As shown in Figure 2.8, the application of an electric field induces the separation of adjacent particles. This observation indicates a hydrodynamic repulsion between the particles resulted from the extensile EHD flow. If the EHD flow is contractile, we would have instead observed particles' aggregation into close-packed crystals.[39] Therefore, our experiments are consistent with the computational results shown in Figures 2.7a and 2.7b with the experimentally measured zeta potentials.

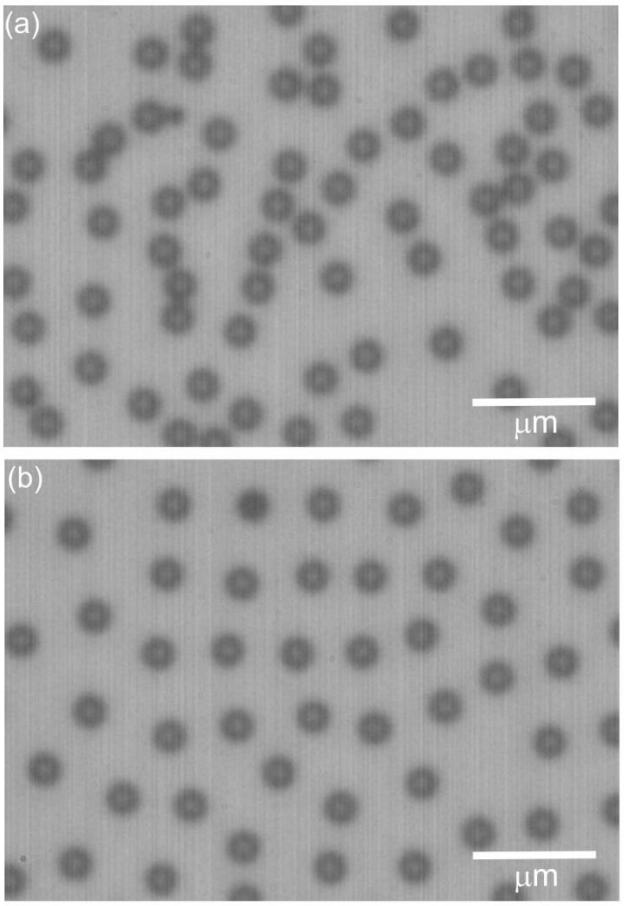

Figure 2.8. Optical images (a) before and (b) after an AC electric field (V_{pp} = 7 volts and f_E = 1300 Hz) is applied. The segregation of colloidal particles upon the field application indicates extensile EHD flow around them.

After validating our simulation method for a single magnetic microsphere, we further simulated a tilted linear chain assembled from five monomers. To avoid numerical singularity, we keep a small gap of 50 nm between neighboring monomers. Eq. (3.3) – (3.13) still applies, but we enlarged our simulation box to $60R \times 30R$ to ensure that the electric field far from the chain remains unperturbed. Figure 2.9a shows the real part of the electric potential, Re(ψ), around a pentamer with $\theta_c = 60°$. Since our particles are positively polarized, the equipotential lines are tangential to each of them. The potential on the electrode increases as one moves away from the chain. However, unlike an isolated sphere, the potential distribution around the tilted chain is no longer symmetric: it increases faster on the chain's left side than the right side. Since the tangential

potential gradient $\nabla_t \psi$ directly influences the slip velocity via Eq. (2.11), the EHD flow around a tilted chain is also asymmetric. As shown in Figure 2.9b, the extensile EHD flow is much stronger on the left side of the chain. Such an unbalanced electric potential and EHD flow will generate finite Maxwell and hydrodynamic stresses. Upon integration of both stresses along the chain surface, we can obtain the net force acting on the chain,

$$\begin{aligned} \mathbf{F}_{\mathrm{E}} &= \int \varepsilon_0 \varepsilon_m \left(\langle \mathbf{E}\mathbf{E} \rangle - \frac{1}{2} \langle E^2 \rangle \mathbf{I} \right) \cdot \hat{\mathbf{n}} dS \\ \mathbf{F}_{\mathrm{H}} &= \int \left[-p\mathbf{I} + \mu \left(\nabla \mathbf{u} + \nabla \mathbf{u}^{\mathrm{T}} \right) \right] \cdot \hat{\mathbf{n}} dS \end{aligned}, \tag{2.14}$$

where $\hat{\mathbf{n}}$ is the particle surface normal. For parameters used in Table 1 and Figure 2.9, we obtain $F_{\mathrm{y}} = F_{\mathrm{E,y}} + F_{\mathrm{H,y}} = 2.00 \times 10^{-13}$ N and $F_{\mathrm{z}} = F_{\mathrm{E,z}} + F_{\mathrm{H,z}} = -1.81 \times 10^{-12}$ N. This indicates that the chain will translate along the positive *y*-direction, consistent with our experimental observation. Moreover, the extensile flow also induces a downward force (negative F_z) that reorients the chain further towards the substrate. Therefore, the COMSOL calculations confirm our hypothesis that an unbalanced extensile EHD flow around a tilted chain causes both its lateral translation and re-orientation towards the substrate. Both are non-trivial effects generated by the superimposed AC electric field.

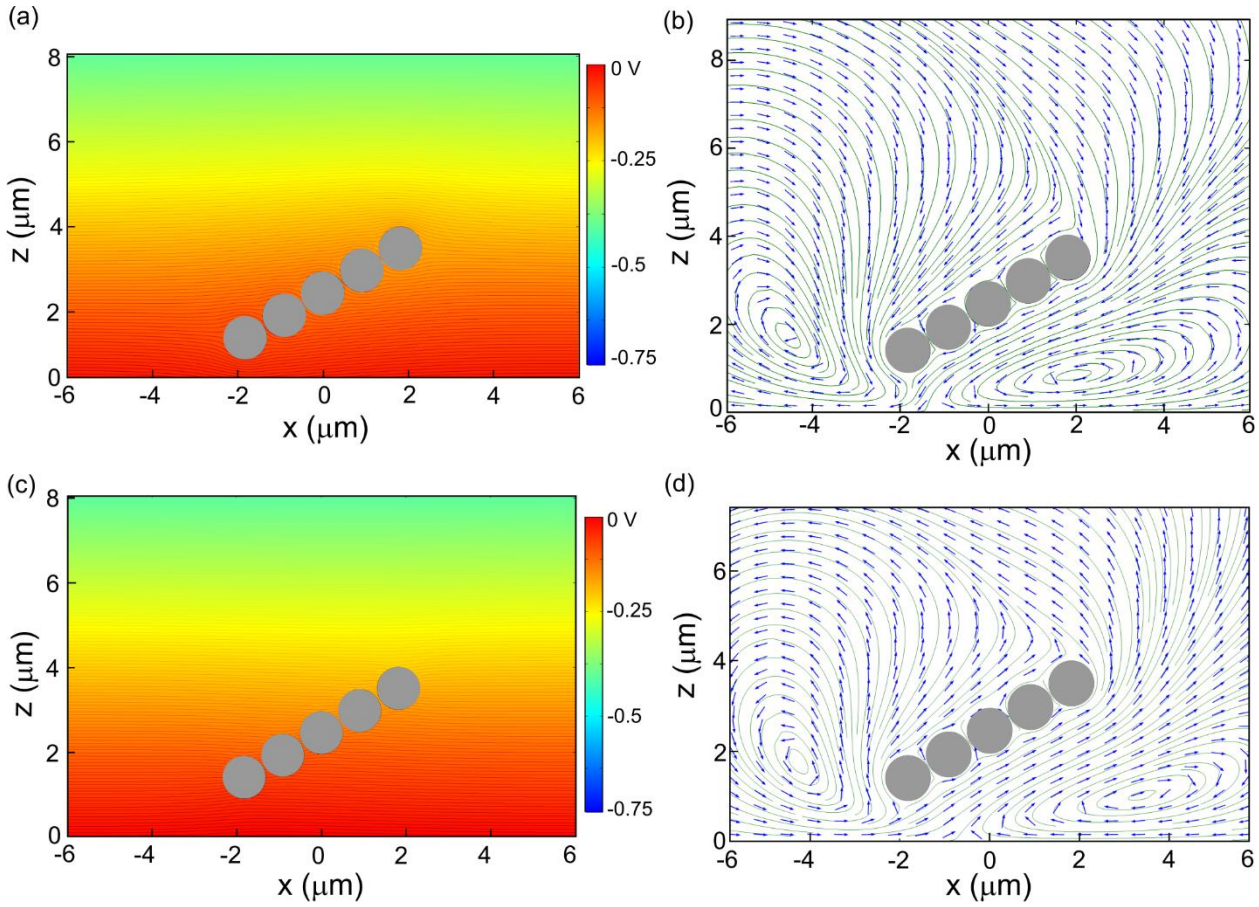

Figure 2.9 (a) The real part of the electric potential, Re(ψ), around a pentamer chain consisting of 1 μm magnetic microspheres (ζ = -60 mV) near an electrode. (b) The streamlines for its associated EHD flow. (c) The real part of the electric potential, Re(ψ), around a pentamer chain consisting of 1 μm magnetic microspheres (ζ = -20 mV) near an electrode. (d) The streamlines for its associated EHD flow. All other parameters are listed in Table 2.1.

If we model the linear chain as a rod of aspect ratio *L*/2*R*, its drag coefficients parallel and perpendicular to the chain are[47-48]

$$\begin{aligned} \zeta_{\parallel} &= \frac{2\pi\mu L}{\ln\left(L/2R\right)-0.114} \\ \zeta_{\perp} &= \frac{4\pi\mu L}{\ln\left(L/2R\right)+0.886} \end{aligned} . \tag{2.15}$$

We can further calculate the translation speed, U_c, of a linear chain along the *y*-direction:

$$U_c = F_y \sin^2\theta_c / \zeta_{\parallel} + F_y \cos^2\theta_c / \zeta_{\perp} . \tag{2.16}$$

Figure 2.10 shows the impact of chain angle θ_c on its translation speed U_c. Consistent with our experimental observation, the linear chain does not translate when it is perfectly horizontal or vertical because of its symmetry in electric potential distribution and EHD flow. Whenever the symmetry is broken for a tilted chain, a net translation ensues. The maximum velocity occurs when the chain is tilted ~ 70°, different from ~ 45° in experiments. We note, however, that our numerical simulation is only in two dimensions. Therefore, we cannot directly compare our calculation results with the experimentally measured velocities. Nonetheless, the non-monotonic dependence of translation speed on the chain angle, the order-of-magnitude consistency on the chain propulsion speed, the correct chain propulsion direction, and re-orientation of the chain towards the substrate upon the application of electric field have all been reproduced in our simulation. These results provide strong support to our explanation of the experimental observation. A full 3D simulation will be performed in the near future for detailed quantitative comparison.

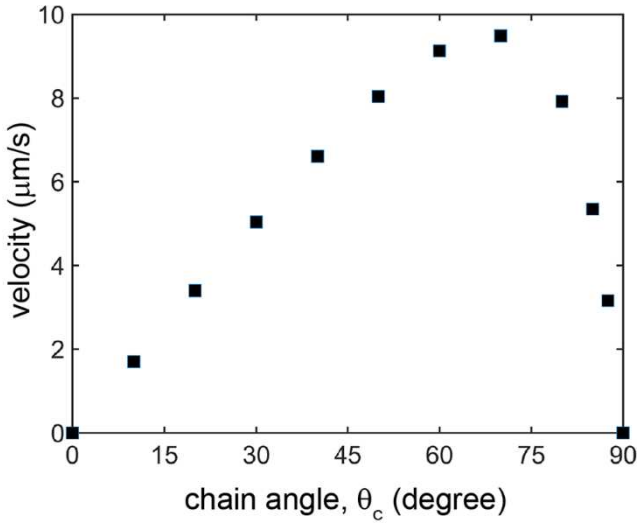

Figure 2.10 The dependence of chain translation velocity U_c on chain angle θ_c based on numerical calculation. All parameters are listed in Table 1.

2.6 Conclusions

Using two-dimensional magnetic fields, we assembled colloidal microspheres into linear chains that are tilted with respect to the substrate. The chain orientation can be tuned conveniently by the relative magnetic field strengths along two orthogonal directions. A superimposed AC electric field applied perpendicular to the substrate induces chain translation because of an unbalanced electrohydrodynamic flow surrounding the tilted chain. We also performed numerical computations that correctly capture the impact of the electric field on the chain orientation, chain propulsion direction, and the dependence of translation speed on the chain tilting angle. Instead of focusing on the design of complex-shaped microbots, our work shows that one can steer microbots assembled from simple isotropic building blocks. When lying on a substrate, our chains are symmetric fore and aft. However, the symmetry of hydrodynamic flow is broken by manipulating their relative orientation to the substrate. Although studied with a simple chain geometry, the demonstrated mechanism here can be applied to other types of synthetic microbots, thus spurring a new dimension to control the propulsion of microscopic objects.

Acknowledgement

This work is supported by National Science Foundation (CBET-1805073).

References

1. Purcell, E. M., Life at low Reynolds number. *American journal of physics* **1977,** *45*, 3-11.

2. Yang, T.; Sprinkle, B.; Guo, Y.; Qian, J.; Hua, D.; Donev, A.; Marr, D. W.; Wu, N., Reconfigurable microbots folded from simple colloidal chains. *Proceedings of the National Academy of Sciences* **2020,** *117*, 18186-18193.

3. Buttinoni, I.; Bialké, J.; Kümmel, F.; Löwen, H.; Bechinger, C.; Speck, T. J. P. r. l., Dynamical clustering and phase separation in suspensions of self-propelled colloidal particles. **2013,** *110*, 238301.

4. Howse, J. R.; Jones, R. A.; Ryan, A. J.; Gough, T.; Vafabakhsh, R.; Golestanian, R., Self-motile colloidal particles: from directed propulsion to random walk. *Physical review letters* **2007,** *99*, 048102.

5. Paxton, W. F.; Baker, P. T.; Kline, T. R.; Wang, Y.; Mallouk, T. E.; Sen, A., Catalytically induced electrokinetics for motors and micropumps. *Journal of the American Chemical Society* **2006,** *128*, 14881-14888.

6. Gangwal, S.; Cayre, O. J.; Bazant, M. Z.; Velev, O. D., Induced-charge electrophoresis of metallodielectric particles. *Physical review letters* **2008,** *100*, 058302.

7. Jiang, H.-R.; Yoshinaga, N.; Sano, M., Active motion of a Janus particle by self-thermophoresis in a defocused laser beam. *Physical review letters* **2010,** *105*, 268302.

8. Chen, J.; Zhang, H.; Zheng, X.; Cui, H. J. A. A., Janus particle microshuttle: 1D directional self-propulsion modulated by AC electrical field. **2014,** *4*, 031325.

9. Paxton, W. F.; Sundararajan, S.; Mallouk, T. E.; Sen, A. J. A. C. I. E., Chemical locomotion. **2006,** *45*, 5420-5429.

10. Wang, S.; Ma, F.; Zhao, H.; Wu, N. J. A. a. m.; interfaces, Bulk synthesis of metal–organic hybrid dimers and their propulsion under electric fields. **2014,** *6*, 4560-4569.

11. Ni, S.; Marini, E.; Buttinoni, I.; Wolf, H.; Isa, L. J. S. M., Hybrid colloidal microswimmers through sequential capillary assembly. **2017,** *13*, 4252-4259.

12. Shields IV, C. W.; Han, K.; Ma, F.; Miloh, T.; Yossifon, G.; Velev, O. D. J. A. F. M., Supercolloidal spinners: Complex active particles for electrically powered and switchable rotation. **2018,** *28*, 1803465.

13. Brooks, A. M.; Tasinkevych, M.; Sabrina, S.; Velegol, D.; Sen, A.; Bishop, K. J. J. N. c., Shape-directed rotation of homogeneous micromotors via catalytic self-electrophoresis. **2019,** *10*, 495.

14. Wang, Z.; Wang, Z.; Li, J.; Cheung, S. T. H.; Tian, C.; Kim, S.-H.; Yi, G.-R.; Ducrot, E.; Wang, Y. J. J. o. t. A. C. S., Active patchy colloids with shape-tunable dynamics. **2019,** *141*, 14853-14863.

15. Lee, J. G.; Brooks, A. M.; Shelton, W. A.; Bishop, K. J. M.; Bharti, B., Directed propulsion of spherical particles along three dimensional helical trajectories. *Nature Communications* **2019,** *10*, 2575.

16. Xie, H.; Sun, M.; Fan, X.; Lin, Z.; Chen, W.; Wang, L.; Dong, L.; He, Q., Reconfigurable magnetic microrobot swarm: Multimode transformation, locomotion, and manipulation. *Science Robotics* **2019,** *4*.

17. Medina-Sánchez, M.; Magdanz, V.; Guix, M.; Fomin, V. M.; Schmidt, O. G., Swimming microrobots: Soft, reconfigurable, and smart. *Advanced Functional Materials* **2018,** *28*, 1707228.

18. Xin, C.; Jin, D.; Hu, Y.; Yang, L.; Li, R.; Wang, L.; Ren, Z.; Wang, D.; Ji, S.; Hu, K., Programmable shape-morphing microrobots for localized cancer cells treatment. **2021**.

19. Gao, W.; Dong, R.; Thamphiwatana, S.; Li, J.; Gao, W.; Zhang, L.; Wang, J., Artificial micromotors in the mouse's stomach: A step toward in vivo use of synthetic motors. *ACS nano* **2015,** *9*, 117-123.

20. Gao, W.; Wang, J., The environmental impact of micro/nanomachines: a review. *Acs Nano* **2014,** *8*, 3170-3180.

21. Moo, J. G. S.; Pumera, M., Chemical energy powered nano/micro/macromotors and the environment. *Chemistry–A European Journal* **2015,** *21*, 58-72.

22. Parmar, J.; Ma, X.; Katuri, J.; Simmchen, J.; Stanton, M. M.; Trichet-Paredes, C.; Soler, L.; Sanchez, S., Nano and micro architectures for self-propelled motors. *Science and technology of advanced materials* **2015,** *16*, 014802.

23. Fan, D.; Yin, Z.; Cheong, R.; Zhu, F. Q.; Cammarata, R. C.; Chien, C. L.; Levchenko, A., Subcellular-resolution delivery of a cytokine through precisely manipulated nanowires. *Nat. Nanotechnol* **2010,** *5*, 545-551.

24. Fischer, P.; Ghosh, A., Magnetically actuated propulsion at low Reynolds numbers: Towards nanoscale control. *Nanoscale* **2011,** *3*, 557-563.

25. Hong, Y.; Diaz, M.; Córdova-Figueroa, U. M.; Sen, A., Light-driven titanium-dioxide-based reversible microfireworks and micromotor/micropump systems. *Adv. Funct. Mater* **2010,** *20*, 1568-1576.

26. Li, J.; Angsantikul, P.; Liu, W.; de Avila, B. E. F.; Chang, X.; Sandraz, E.; Liang, Y.; Zhu, S.; Zhang, Y.; Chen, C., Biomimetic platelet-camouflaged nanorobots for binding and isolation of biological threats. *Adv. Mater* **2018,** *30*, 1704800.

27. Li, J.; de Avila, B. E. F.; Gao, W.; Zhang, L.; Wang, J., Micro/nanorobots for biomedicine: Delivery, surgery, sensing, and detoxification. *Sci. Robot* **2017**.

28. Lin, Z.; Si, T.; Wu, Z.; Gao, C.; Lin, X.; He, Q., Light-activated active colloid ribbons. *Angew. Chem. Int. Ed* **2017,** *56*, 13517-13520.

29. Palacci, J.; Sacanna, S.; Vatchinsky, A.; Chaikin, P. M.; Pine, D. J., Photoactivated colloidal dockers for cargo transportation. *J. Am. Chem. Soc* **2013,** *135*, 15978-15981.

30. Wang, J., Can Man-Made Nanomachines Compete with Nature Biomotors? *ACS Nano* **2009,** *3*, 4-9.

31. Wang, W.; Li, S.; Mair, L.; Ahmed, S.; Huang, T. J.; Mallouk, T. E., Acoustic propulsion of nanorod motors inside living cells. *Angew. Chem. Int. Ed 2014*, 3201-3204.

32. Rao, Q.; Si, T.; Wu, Z.; Xuan, M.; He, Q., A Light-activated explosive micropropeller. *Sci. Rep* **2017,** *7*, 4621.

33. Zhou, D.; Gao, Y.; Yang, J.; Li, Y. G. C.; Shao, G.; Zhang, G.; Li, T.; Li, L., Light-Ultrasound driven collective "Firework". *Behavior of Nanomotors. Adv. Sci* **2018,** *5*, 1800122.

34. Rasband, W. S., ImageJ.

35. Morgan, H.; Green, N. G., *AC electrokinetics : colloids and nanoparticles*. Research studies press: Philadelphia, PA, 2003.

36. Jones, T. B., *Electromechanics of particles*. Cambridge University Press: 1995.

37. Ku, J.; Liu, X.; Chen, H.; Deng, R.; Yan, Q. J. A. A., Interaction between two magnetic dipoles in a uniform magnetic field. **2016,** *6*, 025004.

38. Hynninen, A.-P.; Dijkstra, M. J. P. r. l., Phase diagram of dipolar hard and soft spheres: Manipulation of colloidal crystal structures by an external field. **2005,** *94*, 138303.

39. Ristenpart, W.; Aksay, I. A.; Saville, D., Electrohydrodynamic flow around a colloidal particle near an electrode with an oscillating potential. *Journal of Fluid Mechanics* **2007,** *575*, 83.

40. Ristenpart, W.; Aksay, I. A.; Saville, D., Assembly of colloidal aggregates by electrohydrodynamic flow: Kinetic experiments and scaling analysis. *Physical Review E* **2004,** *69*, 021405.

41. Ma, F.; Wang, S.; Wu, D. T.; Wu, N., Electric-field–induced assembly and propulsion of chiral colloidal clusters. *Proceedings of the national academy of sciences* **2015,** *112*, 6307-6312.

42. Ma, F.; Yang, X.; Zhao, H.; Wu, N., Inducing propulsion of colloidal dimers by breaking the symmetry in electrohydrodynamic flow. *Physical review letters* **2015,** *115*, 208302.

43. Yariv, E.; Schnitzer, O., Electrokinetic particle-electrode interactions at high frequencies. *Physical Review E* **2013,** *87*, 012310.

44. Oostendorp, T. F.; van Oosterom, A., The surface laplacian of the potential: theory and application. *IEEE Transactions on Biomedical Engineering* **1996,** *43*, 394-405.

45. Yang, X.; Johnson, S.; Wu, N., The Impact of stern-layer conductivity on the electrohydrodynamic flow around colloidal motors under an alternating current electric field. *Advanced Intelligent Systems* **2019,** *1*, 1900096.

46. Nakano, M.; Ding, Z.; Suehiro, J., Comparison of sensitivity and quantitation between microbead dielectrophoresis-based DNA detection and real-time PCR. *Biosensors* **2017,** *7*, 44.

47. Broersma, S., Viscous force and torque constants for a cylinder. *The Journal of Chemical Physics* **1981,** *74*, 6989-6990.

48. Yang, K.; Lu, C.; Zhao, X.; Kawamura, R., From bead to rod: Comparison of theories by measuring translational drag coefficients of micron-sized magnetic bead-chains in Stokes flow. *PloS one* **2017,** *12*, e0188015.

CHAPTER 3

ASSEMBLY OF MAGNETIC MICROSPHERES UNDER ORTHOGONALLY APPLIED MAGNETIC AND ELECTRIC FIELDS

3.1 Abstract

With control over both space and time, colloidal structures can be used as either model systems for directed assembly or functional optical or electrical materials. Previous work mainly focused on the assembly of colloids under specific external fields where controlling the field-particle interaction is crucial. Arguably, it is difficult to control the orientational states and achieve local periodicity under any time-varying modulations. Here, we take advantage of both electric and magnetic fields where almost all types of particles can be responsive to the electric field due to a mismatch in dielectric and conductive properties between particles and solvent, while magnetic fields can be conveniently manipulated in three dimensions. We applied two fields orthogonally to magnetic microsphere suspensions, which allowed us to independently tune both the magnitude and direction of dipolar attraction and repulsion between the particles. As a result, we obtained a high density of well-aligned but individually separated long stripes at low and intermediate particle concentrations. The inter- and intra-stripe spacings were tuned by adjusting the particle concentration and relative field strengths of both fields. At high particle concentrations, the microspheres were assembled into small clusters such as trimers, tetramers, heptamers, and nonamers under the electric field due to the synergy between dipolar interaction and electrohydrodynamic flow. Those clusters, as unique building blocks, were subsequently assembled into hierarchical structures by superimposing a one-dimensional magnetic field. Overall, we present a method to reach equilibrium states of global configurations with controllable periodicity via competing dipolar attractions and repulsions. Our results demonstrate the potential

in using combined fields to make diversified types of highly aligned structures for applications in high strength composites, optical materials, or structured battery electrodes.

3.2 Introduction

Colloidal assembly, with control over space and time, can remarkably enrich their prospects of fabricating functional optical, electrical, and magnetic materials[1-3] or forming model systems to answer fundamental scientific questions.[4] Even crystalline arrangement of colloids in one (1D) and two dimensions (2D) have seen a wide range of applications such as security identification,[4] sensing and displays,[5] surface modifications,[6-7] and rheological fluids.[8] Although computations have been advanced enough to predict the colloidal configuration required for exhibiting specific material properties,[9] experimental realizations are typically constrained by available means to tailor particle size, shape, orientation, and interactions that lead to those structures. For example, although dipolar electric or magnetic interactions are pervasive in directed assembly under external fields, there is no easy route to independently control dipolar attraction and repulsion since both of them depend on the angle between the particles center-to-center separation vector and the applied field direction. Moreover, complex building blocks such as particles with anisotropic shape, surface properties, or chemical compositions are challenging to make.

Herein, we combined 1D AC magnetic field parallel to the substrate and 1D AC electric field perpendicular to the substrate for colloidal assembly. By inducing two mutually orthogonal electric and magnetic dipoles on the same particle, we precisely controlled the magnitude and direction of dipolar attraction and repulsion independently. In addition, by tuning the electric field frequency, we can vary the initial building blocks from simple monomers to clusters of trimers,

tetramers, heptamers, and nonamers. As a result, various well-defined structures with increasing complexity were fabricated under the combined electric and magnetic fields.

3.3 Experimental Methods

Materials. Composite magnetic particles of different sizes such as Dynabeads® MyOne™ Carboxylic Acid (1 μm in diameter), Dynabeads® M-270™ Carboxylic Acid (2.7 μm in diameter) were purchased from Thermo Fisher Scientific (Waltham, MA). Indium-tin-oxide (ITO) glass slides (15-25 Ω per sq) were purchased from Sigma-Aldrich. Polyester films were purchased from Micron Wings. Solvents such as acetone and isopropanol were purchased from Pharmco. Poly(sodium 4-styrene sulfonate) (molecular weight = 70,000) was purchased from Sigma-Aldrich.

Experimental Setup. Our experimental setup is shown in Figure 3.1. We used two ITO glass slides as the bottom and top electrodes. A 100-μm thick non-conducting polyester film was used as the spacers, forming a chamber between two electrodes. In a typical experiment, 5-10 μL of dilute Dynabeads® solution was added. To prevent particles from sticking to ITO electrodes, we treated them in the following ways. First, we cleaned the ITO glass with acetone and isopropanol for 15 minutes inside an ultrasonic bath. They were then treated under oxygen plasma for one minute, making them hydrophilic. Finally, they were coated with aqueous poly(sodium 4-styrene sulfonate) solution (5 mg/mL) to bear negative surface charges. As a result, the carboxyl-functionalized particles experience electrostatic repulsion from the electrode. We applied an AC electric field between two ITO glasses via an AC function generator (RIGOL DS1054Z). The range of AC electric voltage applied is 0-10 volts in peak value, and frequency, f_E, is between 500 Hz and 1 MHz. The magnetic field energy sources consist of four air-cored copper solenoid coils

of 50 mm inner diameter, 51 mm length, and 400 turns with a current capacity of 3.5A. This setup allowed us to incorporate 2D magnetic fields by arranging the four coils orthogonally in the *x*-*y* plane. Using a custom-made MATLAB program, we applied the magnetic field with variable strengths, frequencies, and phase angles. Experimental observations were captured in static images and real-time movies using an inverted optical microscope (Olympus IX71) with a black-and-white camera (EPIX SV643M).

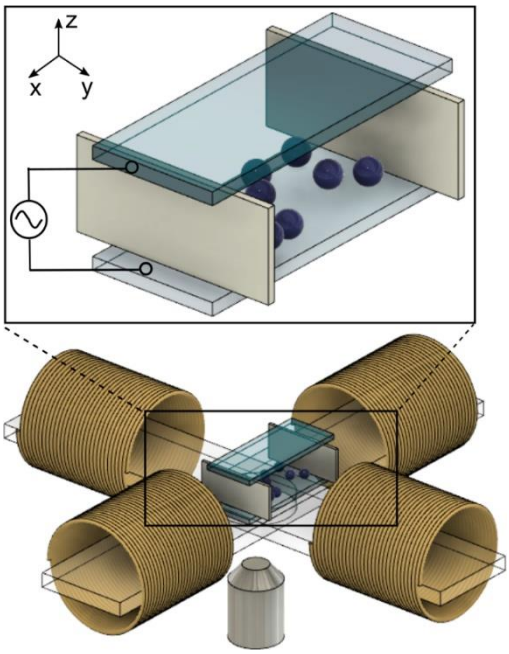

Figure 3.1 Schematic of the experimental setup using combined electric (in the z-direction) and magnetic fields (in x- and y-direction). The range of the applied electric field is 0-10 volts in peak values across a 100 μm gap and 500 Hz -1 MHz. And the range of the applied magnetic field is 0 -16 mT and 50 Hz.

Diffraction patterns. We first extracted centroids of particles from the optical images using a custom-written Matlab code. An appropriate thresholding value was chosen for better illumination of individual elements inside optical images. The noises were removed by filling appropriate holes as a part of shape-based filtering. Finally, the centroid of each particle was extracted. For particles

that are in close contact, the peripherals were eroded before their centroids were identified. To calculate the associated diffraction patterns, we evaluated the real part of the structure factor

$$S(\mathbf{k}) = \frac{1}{N}\sum_{i=0}^{N-1}\sum_{j=0}^{N-1}\exp\left[2\pi i\mathbf{k}\cdot(\mathbf{r}_j - \mathbf{r}_i)\right], \tag{3.1}$$

where $\mathbf{k}$ is the wavevector and $\mathbf{r}_i$ is the position vector of particle *i*. From the diffraction patterns, we can further obtain the estimation of both inter- and intra-stripe spacings.

3.4 Results and Discussion

One dimensional magnetic or electric field has been widely used to align fillers such as nanospheres, nanotubes, or platelets into linear chains and fibers in composite materials to enhance their mechanical strengths.[10-11] They have also been used to tune the structure and flow properties of magnetorheological or electrorheological fluids.[12] The obtained nanostructures are, however, not well-controlled. For example, although nanoparticles can be aligned into individual linear chains at low particle concentrations due to induced dipolar attractions, the assembled chains tend to aggregate further into bundles at intermediate and high particle concentrations, as shown in Figure 3.2a when we applied a uniaxial magnetic field $\mathbf{B} = B_{\mathrm{y}}\cos(2\pi f_{\mathrm{M}}t)\hat{\mathbf{y}}$ along the *y*-direction. This phenomenon can be understood by considering two linear colloidal chains adjacent to each other (Figure 3.2b). While there is a strong dipolar repulsion between the chains separated side by side, the total energy can be minimized by staggering two chains together. Therefore, there is a strong driving force for the aggregation of neighboring chains until those bundles are separated wide enough that the dipolar force between them is weak. Usually, this process depends sensitively on the local concentration of chains. As a result, the inter-chain spacings exhibit a wide distribution.

On the other hand, when we apply a one-dimension AC electric field along the z-direction to the same microspheres, we obtained a non-close-packed hexagonal crystal of particles due to

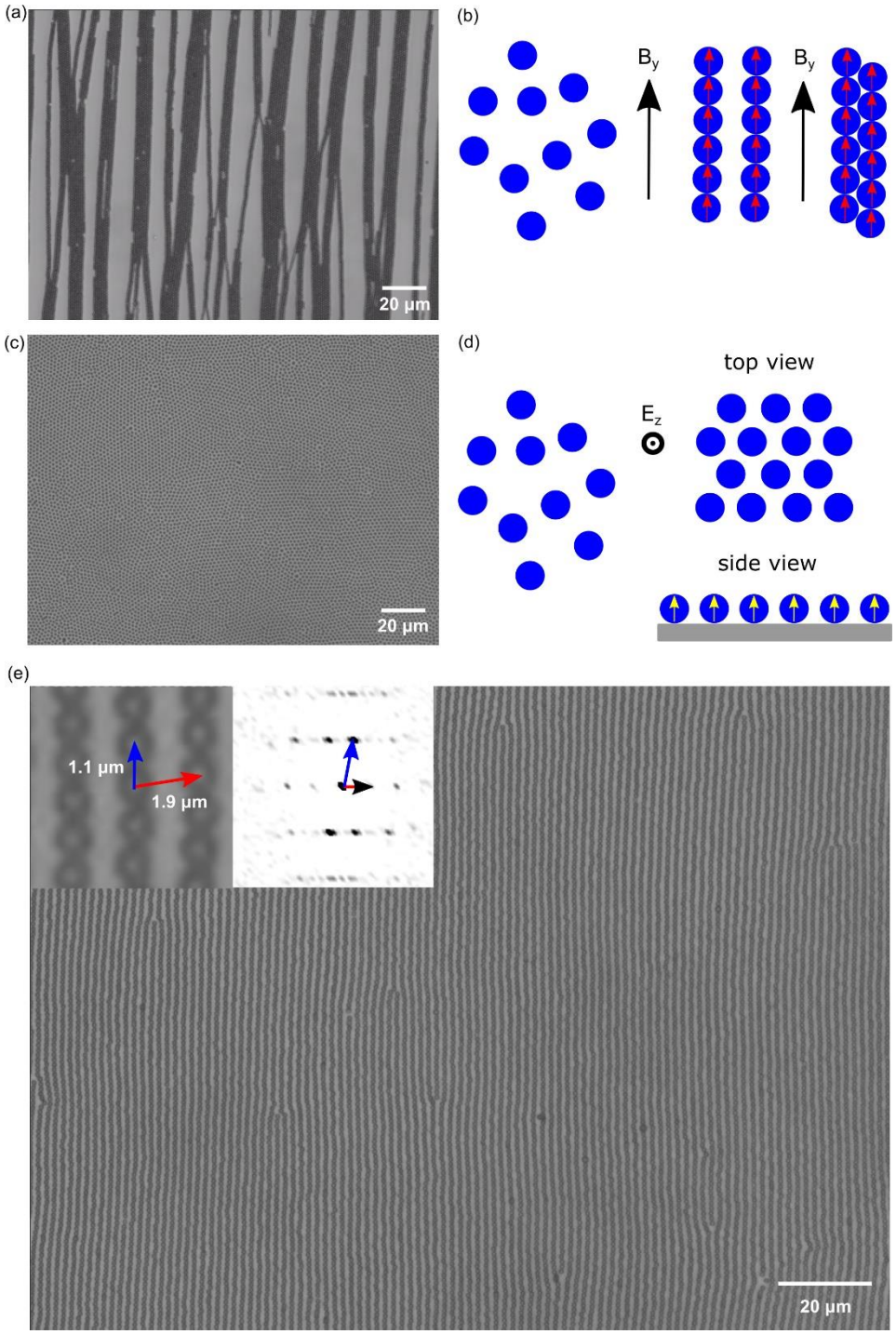

Figure 3.2 Colloidal monolayers assembled under magnetic and electric fields. (a) Optical image of the bundles of linear chains formed by one-dimensional AC magnetic field along the y-direction. B_y = 4.25 mT and f_M = 50 Hz. (b) Schematic showing the assembly of microspheres into linear

chains and bundles. Red arrows indicate the induced magnetic dipoles. (c) Optical image of the non-close-packed hexagonal array formed under an AC electric field along the z-direction ($E_{z,rms}$ = 7.07×10^4 V/m and at f_E = 1,300 Hz). (d) Schematic showing the assembly of microspheres into hexagonal arrays. Yellow arrows indicate the induced electric dipoles. (e) Optical image of high density and well-aligned colloidal chains when the magnetic and electric fields are superimposed. The insets show a magnified area of the chains and the diffraction pattern of the whole image.

strong dipolar repulsions between them (Figures 3.2c and 3.2d). Interestingly, when we combine these two fields, we obtain highly concentrated and well-aligned stripes shown in Figure 3.2e. Instead of bundling together, those chains remain closely separated. From the image's diffraction pattern (inset of Figure 3.2e), we can obtain the separations between nearest neighbors in two different directions. Such a densely packed stripe structure cannot be achieved by individual fields only, demonstrating the advantage of combining two fields.

We can make this kind of structure because we separately control the amplitude and direction of dipolar attraction and repulsion via the combined magnetic and electric fields, which generate two orthogonally aligned dipoles. Since the magnetic field is along the y-direction, the induced magnetic dipole on each particle points toward the same direction. The head-to-tail attraction between magnetic dipoles is the driving force for stripe formation. However, a side effect is that neighboring stripes also feel a driving force to reduce the total energy by staggering together. We resolve this issue by inducing an electric dipole on each particle orthogonal to the magnetic dipole via a perpendicular electric field. As a result, all particles feel a uniform shoulder-to-shoulder electric dipolar repulsion among themselves along the substrate. This force is weak enough not to interfere with the magnetic alignment of individual stripes. Still, it is strong enough to prevent the aggregation of neighboring stripes, leading to the pattern shown in Figure 3.2e.

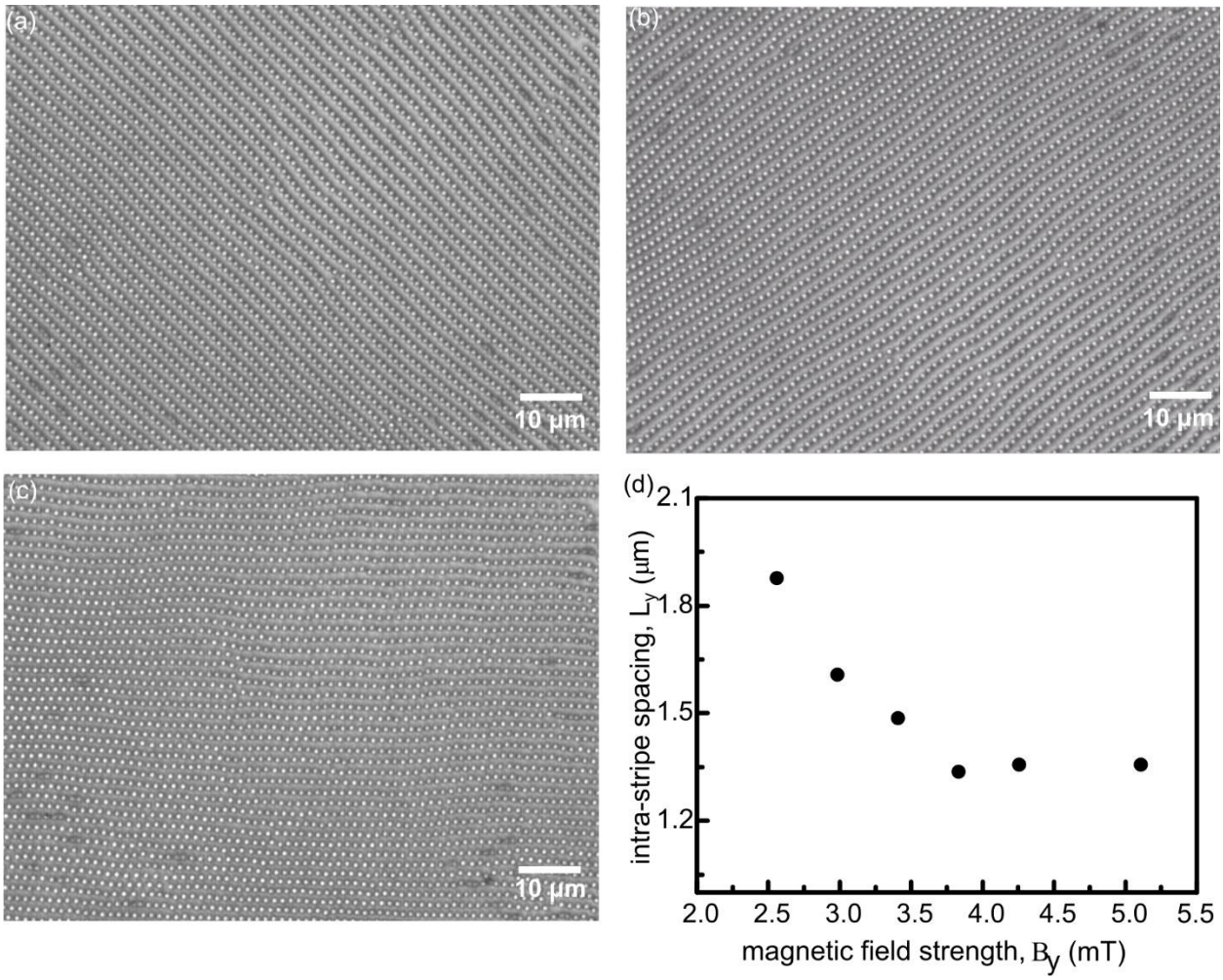

Figure 3.3 The impact of magnetic field on stripe patterns. The optical images illustrating the chain orientation at different magnetic field conditions. (a) B_x = 4.25 mT and B_y = 4.25 mT. (b) B_x = 4.25 mT and B_y = 4.25 mT, and (c) B_x = 4.25 mT and B_y = 0 mT. (d) The intra-stripe spacing, L_y, can be tuned by the magnetic field strength. The electric field is held constant at $E_{z,rms} = 7.07\times10^4$ V/m and at f_E = 1,300 Hz.

We further investigated how both fields can control the stripe patterns. First, we show that the applied magnetic field, $\mathbf{B} = B_x \cos(2\pi f_M t)\hat{\mathbf{x}} + B_y \cos(2\pi f_M t + \varphi)\hat{\mathbf{y}}$, can control the chain orientations. As shown in Figures 3.3a-3.3b, when $B_x = B_y$ and φ=0° (or 180°), the chains are oriented 45° (or -45°) relative to the *x*-axis. Horizontally-oriented chains can be obtained when B_y = 0 (Figure 3.3c). Essentially, the chain orientation can be conveniently adjusted by tuning both

field strength (B_x and B_y) and phase angle (φ) between the magnetic fields in *x*- and *y*-directions. In fact, the response to induced dipoles is quick enough to synchronize with the switch of magnetic field directions where the structural rigidity of stripes is maintained. Furthermore, the intra-chain spacing (L_y), i.e., the separation between neighboring particles along the same chain, can be tuned by the field strength (Figure 3.3d). The magnetic dipolar interaction is proportional to the field strength squared. A stronger dipolar force leads to smaller intra-chain spacing until it reaches a plateau where the double-layer repulsion between neighboring particles balances the magnetic force.

The inter-stripe (L_x) separations can also be tuned by changing the initial particle concentration. Here we define the particle surface coverage $\rho = N\pi a^2 / A$, where N is the number of particles within a field-of-view area A and a is the particle radius. As shown in Figure 3.4, with increasing particle surface coverage, the inter-stripe spacing decreases under the same magnetic and electric field conditions. However, the spacing cannot be reduced below ~ 2 μm when surface coverage is further increased because the microspheres can no longer maintain a monolayer array. Instead, more intriguing patterns emerge, as we will discuss below.

At higher particle concentrations and under a low-frequency AC electric field, we start to observe the assembly of initially randomly distributed particles into smaller and non-planar clusters. For example, at 2,000 Hz, linear trimers in which one central sphere sits on the top of two bottom spheres were observed (Figure 3.5a). Pyramid-like tetramers where one top central sphere associates with three bottom spheres can be found at a lower frequency, e.g., 750 Hz, as shown in Figure 3.5c. The formation of such kinds of oligomers can be attributed to the synergy between dipolar interaction and electrohydrodynamic flow, which has been observed in our previous work[13-14] when we used polystyrene microspheres.

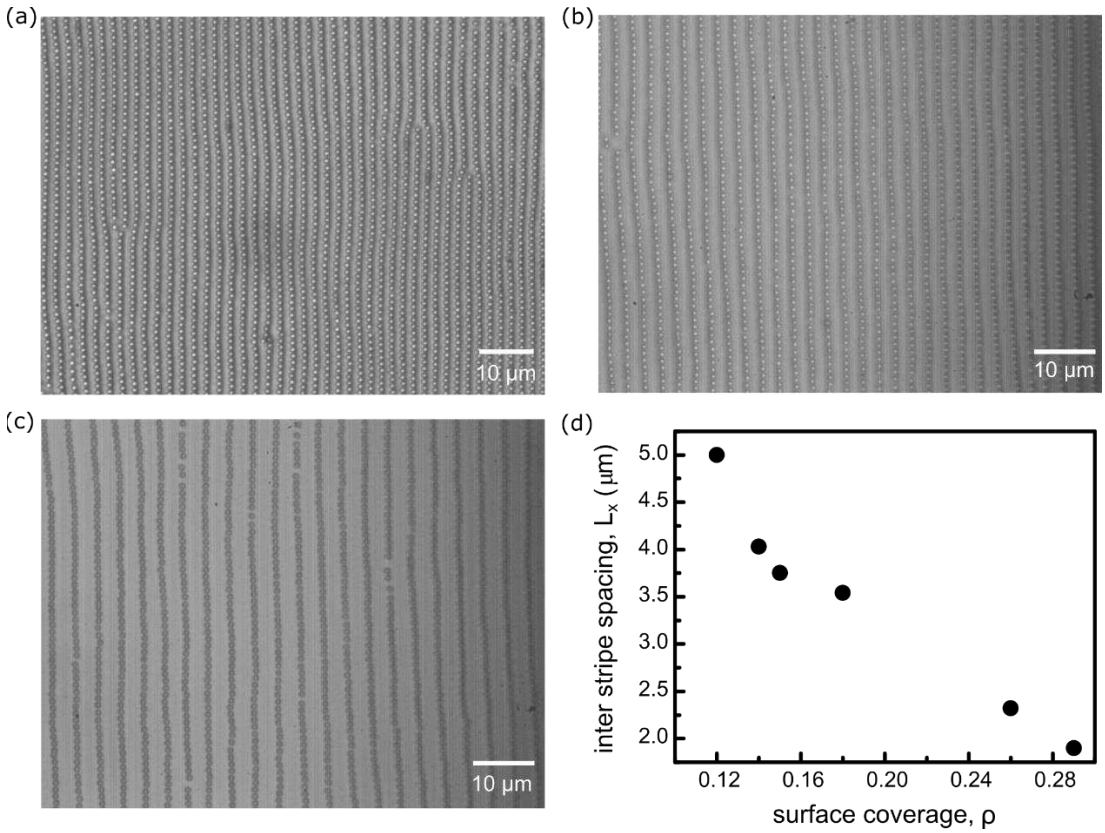

Figure 3.4 Control of the inter-stripe spacing by tuning the particle surface coverage, ρ. Optical images of the stripe pattern at (a) $\rho = 0.28$. (b) $\rho = 0.19$. (c) $\rho = 0.15$. (d) The dependence of the inter-stripe spacing L_x on ρ. $B_y = 4.25$ mT, $f_M = 50$ Hz, $E_{z,rms} = 7.07\times10^4$ V/m, and $f_E = 1{,}300$ Hz.

Since the induced electric dipoles on the particles are perpendicular to the substrate, the dipolar interaction along the substrate is repulsive. So planar clusters would be hard to form. However, there is a tendency for one particle to jump to the top of another due to the head-to-tail dipolar attraction. At low and intermediate particle concentrations, this interaction is weak due to large inter-particle separations. Moreover, there is an energy barrier in switching from dipolar repulsion to attraction since the angle between the particles' center-to-center separation vector and the field vector needs to be less than the magic angle of 54.7°.[15] Although Brownian motion can help lower this energy barrier, it can be significantly reduced by an additional extensile electrohydrodynamic (EHD) flow at low frequencies. The origin and physical explanation of this

EHD flow have been discussed in detail in Chapter 2 and proved to be extensile in nature. Any neighboring particle entrained in this flow (*cf.* Figure 2.7b) will follow the streamlines of a small clockwise vortex, which pushes the particle away from the electrode. This flow allows the neighboring particles to be located at different focus planes and induces their assembly (due to dipolar attraction) into the characteristic non-planar clusters where a central top sphere is associated with multiple bottom spheres. The extensile EHD flow also prevents the formation of linear chains along the electric field direction, although it is a more energetically favorable state from dipolar interaction. Indeed, we did observe vertical chains at frequencies beyond 10 kHz (since the EHD flow is inversely proportional to frequency),[16] where the EHD flow diminishes and dipolar interaction dominates. While our original work in the formation of those colloidal clusters was based on non-magnetic particles, reproducing these architectural building blocks with Dynabeads® here shows the advantage of the electric field where almost all kinds of particles can respond to it as long as there is a mismatch in dielectric constants and conductivities between the particle and medium.

The formation of uniform colloidal clusters such as trimers and tetramers allowed us to study the impacts of combined fields on building blocks beyond microspheres. While the uniformly distributed trimers were randomly oriented under the electric field only, they realigned into trimeric stripes when we superimposed an AC magnetic field along the *y*-direction with their structural rigidity preserved glocally (Figure 3.5b). In comparison, the tetramers can no longer keep their shapes under the 1D magnetic field due to strong magnetic dipolar attraction. They decomposed into trimers and monomers, which arranged alternately into stripes. By using different building blocks assembled by the electric field, we find a route to introduce controlled heterogeneity in the aligned stripes.

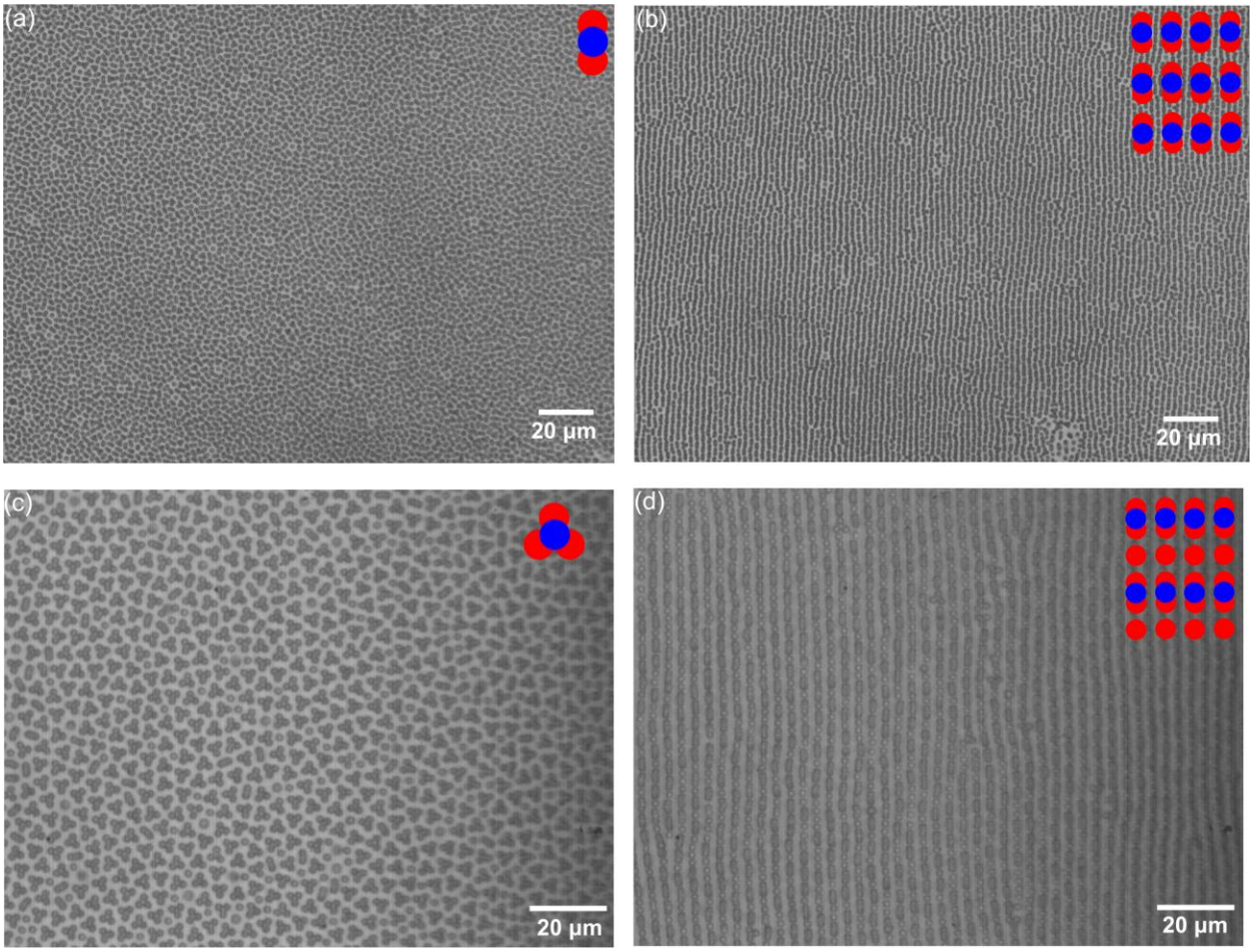

Figure 3.5 Well-aligned chains formed by colloidal trimers and tetramers. (a) Optical image of the linear trimers formed under the electric field only. $E_{z,rms} = 3.54 \times 10^4$ V/m and $f_E = 2000$ Hz. (b) Optical image of the aligned bundles formed by the trimers upon the superposition of a one-dimensional magnetic field. B_y = 5.1 mT. (c) Optical image of the pyramid tetramers formed under the electric field only. at $E_{z,rms} = 2.47 \times 10^4$ V/m and $f_E = 750$ Hz. (d) Optical image of the aligned bundles formed by the tetramers upon the superposition of a one-dimensional magnetic field. B_y = 5.1 mT. Insets show the schematics of the structures. Red spheres are at the bottom plane and blue ones are on the top.

Stripes with finer structures can also be made when we use higher-order building blocks by further decreasing the electric field frequency and increasing the particle concentration. For example, at 450 Hz, two neighboring tetramers assembled into butterfly-like heptamers (by sharing a common vertex) and released one monomer (Figure 3.6a). At an even lower frequency, i.e., 350 Hz, triangular nonamers were formed where three tetramers assembled, and each shared

two of their three vertices with the others (Figure 3.6c). The dependence of cluster size on frequency (i.e., from trimer to nonamer) is consistent with our hypothesis that the extensile EHD flow helps reduce the energy barrier for switching from dipolar repulsion to dipolar attraction between particles located at different focus planes. Since EHD flow is stronger at low frequencies, larger clusters are observed. While the formation of large-size clusters is primarily driven by frequency, we also found that keeping a high particle concentration helped yield as many uniform building blocks as possible within a field of view. This strategy led a favorable kinetic pathway for the assembly of particles into heptamers, nonamers, and even larger clusters.

Just like trimers and tetramers, arrays of heptamers and nonamers reconfigure under the addition of the magnetic field along the *y*-direction. As shown in Figure 3.6b, the heptamers re-orient 90° and connected into wide lanes to maximize the magnetic energy gain. The nonamers, however, become unstable and re-organize into wide lanes consisting of unit cells of rectangular lattices (Figure 3.6d). Arguably, they are equilibrium structures that minimize the sum of magnetic and electric energies. We have also observed the effect of annealing. As time evolved, the fine structures within each lane became more and more uniform.

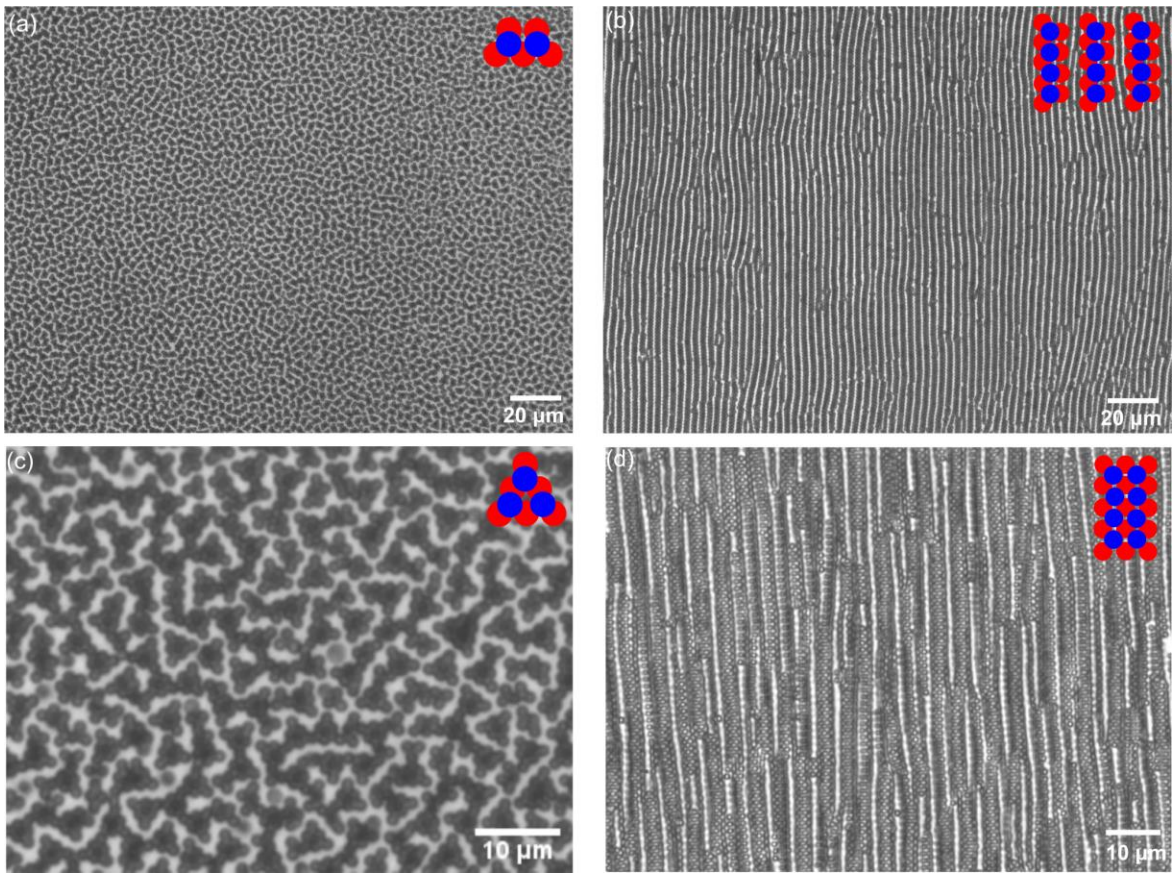

Figure 3.6 Well-aligned lanes formed by colloidal heptamers and nonamers. (a) Optical image of the butterfly-like heptamers formed under the electric field only. $E_z = 1.98 \times 10^4$ V/m and $f_E = 450$ Hz. (b) Optical image of the aligned bundles formed by the heptamers upon the superposition of a one-dimensional magnetic field. $B_y = 5.1$ mT. (c) Optical image of the triangular nonamers formed under the electric field only. $E_z = 1.97 \times 10^4$ V/m and $f_E = 350$ Hz. (d) Optical image of the aligned bundles formed by the nonamers upon the superposition of a one-dimensional magnetic field. $B_y = 5.1$ mT. Insets show the schematics of the structures. Red spheres are at the bottom plane, and blue ones are on the top.

3.5 Conclusions

In this work, we have demonstrated a strategy to control the spatial arrangement of colloidal microspheres by applying both electric and magnetic fields. The combined fields generated orthogonally aligned electric and magnetic dipoles, which allowed us to independently control the magnitude and direction of dipolar attraction and repulsion between particles. As a result, we obtained high-density arrays of well-aligned and individually separated stripes. We have

also assembled the microspheres into new types of building blocks of colloidal oligomers such as linear trimers, pyramid tetramers, butterfly-like heptamers, and triangular nonamers by taking advantage of the synergistic effect of both electric dipolar interaction and electrohydrodynamic flow. Upon the superposition of a one-dimensional magnetic field, we further made stripes and lanes with finer microstructures. Our work demonstrates the interplay of orthogonally aligned electric and magnetic dipoles under combined fields. It paves the route towards making various types of highly aligned structures required in high strength composites, optical materials, or battery electrodes.

Acknowledgment

This work is supported by National Science Foundation (CBET-1805073).

References

1. Smay, J. E.; Cesarano, J.; Lewis, J. A., Colloidal inks for directed assembly of 3-D periodic structures. *Langmuir* **2002,** *18*, 5429-5437.

2. Holtz, J. H.; Asher, S. A., Polymerized colloidal crystal hydrogel films as intelligent chemical sensing materials. *Nature* **1997,** *389*, 829-832.

3. Zaidouny, L.; Bohlein, T.; Roth, J.; Bechinger, C., Periodic average structures of colloidal quasicrystals. *Soft matter* **2014,** *10*, 8705-8710.

4. Wang, W.; Lv, X.; Moran, J. L.; Duan, S.; Zhou, C., A practical guide to active colloids: choosing synthetic model systems for soft matter physics research. *Soft matter* **2020,** *16*, 3846-3868.

5. Ding, T.; Smoukov, S. K.; Baumberg, J. J., Stamping colloidal photonic crystals: a facile way towards complex pixel color patterns for sensing and displays. *Nanoscale* **2015,** *7*, 1857-1863.

6. Wang, X. Inverse colloidal crystal membranes: formation, surface modification and applications. Colorado State University, 2010.

7. Nasilowski, M.; Mahler, B.; Lhuillier, E.; Ithurria, S.; Dubertret, B., Two-dimensional colloidal nanocrystals. *Chemical reviews* **2016,** *116*, 10934-10982.

8. Martin, J. E.; Solis, K. J., Fully alternating, triaxial electric or magnetic fields offer new routes to fluid vorticity. *Soft Matter* **2015,** *11*, 241-254.

9. Ho, K.; Chan, C. T.; Soukoulis, C. M., Existence of a photonic gap in periodic dielectric structures. *Physical Review Letters* **1990,** *65*, 3152.

10. Ignaczak, W.; Sui, X.; Kellersztein, I.; Wagner, H. D.; El Fray, M., The effect of fibre sizing and compatibilizer of polypropylene/poly (butylene terephthalate) blends on the mechanical and interphase properties of basalt fibre reinforced composites. *Polymer International* **2018,** *67*, 414-421.

11. Lin, Z.; Liu, Y.; Raghavan, S.; Moon, K.-s.; Sitaraman, S. K.; Wong, C.-p., Magnetic alignment of hexagonal boron nitride platelets in polymer matrix: toward high performance anisotropic polymer composites for electronic encapsulation. *ACS applied materials & interfaces* **2013,** *5*, 7633-7640.

12. Wen, W.; Huang, X.; Sheng, P., Electrorheological fluids: structures and mechanisms. *Soft Matter* **2008,** *4*, 200-210.

13. Ma, F.; Wu, D. T.; Wu, N., Formation of colloidal molecules induced by alternating-current electric fields. *Journal of the American Chemical Society* **2013,** *135*, 7839-7842.

14. Maestas, J. R.; Ma, F.; Wu, N.; Wu, D. T., Electric-Field-Driven Assembly of Dipolar Spheres Asymmetrically Confined between Two Electrodes. *ACS nano* **2021,** *15*, 2399-2412.

15. Yethiraj, A., Tunable colloids: control of colloidal phase transitions with tunable interactions. *Soft Matter* **2007,** *3*, 1099-1115.

16. Ristenpart, W.; Aksay, I. A.; Saville, D., Electrohydrodynamic flow around a colloidal particle near an electrode with an oscillating potential. *Journal of Fluid Mechanics* **2007,** *575*, 83.

CHAPTER 4

CONCLUSIONS AND FUTURE DIRECTIONS

4.1 Conclusions

The primary goal of this work is to explore the combined impacts of electric and magnetic fields on colloidal assembly and actuation. We exploit the convenience of manipulating multi-axial magnetic fields to control particle orientation and assembly. We also take advantage of the fact that almost all kinds of particles can respond to the electric field and rich electrokinetic phenomena to induce particle motion.

In Chapter 2, we have tried to highlight the importance of exploring new propulsion mechanisms for locomotion of microscopic objects in a low Reynolds number regime. While shape morphing through the swimmer's flexibility is a useful strategy, there are significant challenges associated with objects that do not deform. We decide to control their orientations instead. We assembled magnetic microspheres dispersed randomly in the medium into linear chains. Unlike most common practices of breaking the symmetry of particle shape or surface functionality, we create asymmetry by varying the chain tilt angle relative to the substrate that depends on the relative strength of the magnetic field. This shows a great advantage of narrowing down variables that dictate the dynamics. We find that a superimposed AC electric field induces unbalanced electrohydrodynamic flow on tilted chains and makes them propel along the substrate. We have also performed numerical simulations to successfully predict both chain propulsion direction and the non-monotonic dependence of propulsion speed on the chain tilt angle. Our study provides insights on how combined magnetic and electric fields can tune the orientation and structure of microrobots, which subsequently provides additional control on their propulsion speeds. In this

regard, our proposition of creating a net translation, simply by breaking the fore-aft symmetry through geometric orientation, is a valuable addition to the existing mechanisms.

Chapter 3 demonstrates a new method to make complex colloidal structures from simple building blocks of magnetic microspheres. We apply a 1D AC magnetic field parallel to the substrate and a 1D AC electric field perpendicular to the substrate. As a result, each particle acquires orthogonally aligned magnetic and electric dipoles. This strategy allows us to independently control the magnitude and direction of dipolar attraction and repulsion. As a result, we have obtained a high density of well-aligned and individually separated long stripes at low and intermediate particle concentrations. Furthermore, by changing the electric field frequency at high particle concentration, we have assembled the particles into three-dimensional colloidal clusters of different sizes such as trimers, tetramers, heptamers, and nonamers. As new building blocks, these clusters also respond to the superimposed magnetic field and form thick stripes or lanes with much finer inner microstructures. Our results demonstrate the potential in using combined fields to make highly aligned microstructures necessary in high mechanical strength composites, optical materials, or battery electrodes.

4.2 Future Directions

Since we have worked with the simultaneous application of two different external fields, there are many space and time parameters whose variation or synchronization can create complex effects on colloidal assembly and active motion dynamics. The experiments presented in Chapters 2 and 3 were performed with relatively simple combinations of these two fields. For example, the phase angle between *x*- and *y*- magnetic fields in chapter 2 was zero. In Chapter 3, only a one-dimensional magnetic field was applied. It would be interesting to superimpose more complex

magnetic fields such as rotating or three-dimensional fields with electric fields to study their impacts on the colloidal assembly and actuation.

The mode of microbot propulsion studied in Chapter 2 is based on breaking its symmetry in orientation. A natural question arises on the possibility of using asymmetric actuation of the external fields where the field direction changes in time. For example, a clockwise-counterclockwise rotating magnetic field with equal amplitude and period will generate an equal amount of torque in opposite directions. However, future experiments can be carried out to see whether a net torque can be generated when an ellipsoidal rotating field is applied with unequal periods in the clockwise and counterclockwise directions.

The microstructures obtained in Chapter 3 are intriguing. Although their formation can be explained qualitatively by considering the interplay between magnetic and electric dipolar interactions, we have not systematically studied the impacts of particle concentration and the relative field strengths between the two fields. More importantly, we have observed the re-configuration of pre-formed colloidal clusters such as heptamers and nonamers into higher-order structures upon applying the magnetic fields. While further detailed experimental investigation would be necessary, computations such as Monte Carlo simulations would also provide us new insights into the colloidal interactions. Indeed, our group has performed simulations[1] before reproducing various kinds of crystalline structures assembled under the AC electric field only. Adding a magnetic field is both feasible and necessary to complement our experimental studies.

Currently, our systems consist of one-component colloidal spheres. We performed some preliminary experimental investigation on a binary mixture of magnetic spheres of different sizes and zeta potentials out of curiosity. Important parameters such as the electric polarization coefficient, K, heavily depend on both particle size and zeta potential. Therefore, different

electrokinetic phenomena can be observed on each component even at the same field strength and frequency. Larger particles hardly aggregate because of strong dipolar repulsion between them. Similarly, a weak EHD attraction for smaller particles would prevent them from aggregating as well. Consequently, the mutual interaction between small and large particles can provide a route to making heterogeneous building blocks and some interesting global structures.

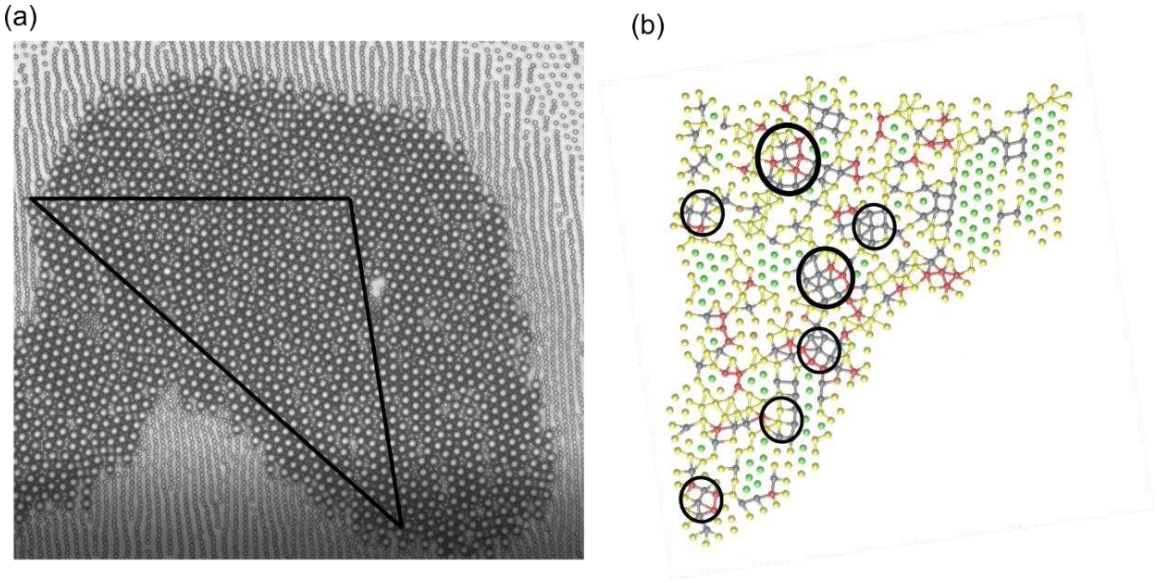

Figure 4.1 $H-lattices$ formed under a system created by the binary mixture of particles(a) Optical images of the cilia-like assembly formed by two different size particles of $2.7\mu m$ and $1\mu m$ under combined electric field and magnetic fields. First, an AC electric field ($E_{z,rms}$ = 3.53×10^4 V/m and at f_E = 2,000 Hz) was applied, and eventually, the frequency was slowly reduced to f_E = 500 Hz that resulted in an island of separated smaller and larger particles. Then a magnetic field $\mathbf{B} = B_x \cos(2\pi f_M t)\hat{\mathbf{x}} + B_y \sin(2\pi f_M t)\hat{\mathbf{y}}$ $f_M = 20Hz$ is applied for t_1. For a time t_2, combined effect of $\mathbf{B}_1 = B_x \cos(2\pi f_M t)\hat{\mathbf{x}} + B_y \sin(2\pi f_M t)\hat{\mathbf{y}}$ and $\mathbf{B}_2 = B_x \cos(2\pi f_M t)\hat{\mathbf{x}} - B_y \sin(2\pi f_M t)\hat{\mathbf{y}}$ was applied, where $B_x \neq B_y$. (b) Characterized by Frank-Kasper local particle environments which are determined by the number and configurations of nearest neighboring particles within a cutoff. Sigma environments are red, H environments are gray, Z environments are green and undefined environments are yellow (represented as a mirror of triangular inset of (a)).

Furthermore, the induced magnetic field from larger particles can influence the local magnetic interaction amongst particles heavily, resulting in layered composites, as seen in Figure 4.1a. Here the system was first driven by an ellipsoidal rotating magnetic field in the anti-clockwise

direction for a period t_1 followed by clockwise rotation for a period t_2. This asymmetric actuation was carried repeatedly with a period of $T = t_1 + t_2$. This could be an interesting way to create a linear and non-linear external modulation by tuning t_1 and t_2 in such a way that t_1 / t_2 is an irrational number.

References

1. Maestas, J. R.; Ma, F.; Wu, N.; Wu, D. T., Electric-field-driven assembly of dipolar spheres asymmetrically confined between two electrodes. *ACS nano* **2021,** *15*, 2399-2412.

2. Heatley, K. L.; Ma, F.; Wu, N., Colloidal molecules assembled from binary spheres under an AC electric field. *Soft matter* **2017,** *13*, 436-444.

3. van der Linden, M. N.; Doye, J. P.; Louis, A. A., Formation of dodecagonal quasicrystals in two-dimensional systems of patchy particles. *The Journal of chemical physics* **2012,** *136*, 054904.

APPENDIX

SUPPLEMNTAL ELECTRONIC FILES

A brief literature reviews about the background of this research is made in Chapter 1. For visual inspection for the readers, the corresponding figures on a particular topic are added. These figures are redrawn with the permission taken from the publishing authority with the help of online platform Copyright Clearance Center RightsLink. As a reference, the statements of permissions are included in supplemental file “Copyright permission”.